The Globular Cluster Luminosity Function and Specific Frequency in Dwarf Elliptical Galaxies[1]

Bryan W. Miller

Gemini Observatory, Casilla 603, La Serena, Chile

Jennifer M. Lotz[2]

National Optical Astronomy Observatory, 950 N. Cherry Ave., Tucson, AZ 85719, USA

ABSTRACT

The globular cluster luminosity function, specific globular cluster frequency, $S_{\rm N}$, specific globular cluster mass, $T_{\rm MP}$, and globular cluster mass fraction in dwarf elliptical galaxies are explored using the full 69 galaxy sample of the *HST* WFPC2 Dwarf Elliptical Galaxy Snapshot Survey. The GCLFs of the dEs are well-represented with a t_5 function with a peak at $M^0_{V,Z}(dE, HST) = -7.3 \pm 0.1$. This is ~ 0.3 magnitudes fainter than the GCLF peaks in giant spiral and elliptical galaxies, but the results are consistent within the uncertainties. The bright-end slope of the luminosity distribution has a power-law form with slope $\alpha = -1.9 \pm 0.1$. The trend of increasing $S_{\rm N}$ or $T_{\rm MP}$ with decreasing host galaxy luminosity is confirmed. The mean value for $T_{\rm MP}$ in dE,N galaxies is about a factor of two higher than the mean value for non-nucleated galaxies and the distributions of $T_{\rm MP}$ in dE,N and dE,noN galaxies are statistically different. These data are combined with results from the literature for a wide range of galaxy types and environments. At low host galaxy masses the distribution of $T_{\rm MP}$ for dE,noN and dI galaxies are similar. This supports the idea that one pathway for forming dE,noN galaxies is by the stripping of dIs. The formation of nuclei and the larger values of $T_{\rm MP}$ in dE,N galaxies may be due to higher star formation rates and star cluster formation efficiencies due to interactions in galaxy cluster environments.

Subject headings: galaxies: dwarf — galaxies: star clusters — galaxies: nuclei

---

[1]Based on observations with the NASA/ESA *Hubble Space Telescope*, obtained at the Space Telescope Science Institute, which is operated by the Association of Universities for Research in Astronomy, Inc., under NASA contract No.NAS5-26555

[2]NOAO Leo Goldberg Fellow

1. Introduction

The properties of the globular cluster (GC) systems of galaxies contain important information about the formation and evolution of the star clusters themselves as well as their host galaxies. In the local universe massive, compact young star clusters that are likely progenitors of traditionally old GCs are usually found in starburst environments such as galaxy mergers (e.g. Holtzman et al. 1992; Miller et al. 1997; Whitmore et al. 1999) or star bursting dwarfs (e.g. Billett et al. 2002; Alonso-Herrero et al. 2004; de Grijs et al. 2005). The metallicity of the gas out of which they form and the time since their formation can be gleaned from the properties of their simple stellar populations. Therefore, massive star clusters are good tracers of significant star forming episodes in their host galaxies. Also, the oldest GCs in the Milky Way have ages consistent with a Hubble time, suggesting that they were among the earliest stellar systems to form and therefore provide us with a window into conditions in the very early universe.

The observed star cluster systems in nearby galaxies are the result of the interplay between the conditions and processes during cluster formation and the processes that destroy clusters. The number of clusters that form in a given potential well depends on the cluster formation efficiency, the cluster formation history, the detailed physics of the cluster formation process, and the initial cluster mass function. All of these factors may be dependent on the initial environmental conditions such as the amount of available gas, the metallicity of the gas, and the external pressure (Fall & Rees 1985; McLaughlin & Pudritz 1996; Elmegreen & Efremov 1997). Star clusters can then be destroyed by a combination of stellar evolution, two-body relaxation, and tidal shocking (e.g. Gnedin & Ostriker 1997; Baumgardt 1998; Fall & Zhang 2001; Vesperini & Zepf 2003). In addition, cluster systems can be both augmented by the accretion of clusters during interactions or mergers and reduced by stripping via strong external tides (Côté et al. 1998; Beasley et al. 2002). Only by studying the properties of star clusters in different environments where different sets of processes may be significant can we constrain our theories of star cluster formation and evolution.

Dwarf galaxies are particularly useful objects for studies of massive star clusters. A census of the globular clusters in Local Group dEs showed that there is a large scatter in the number per galaxy. However, those that do form clusters often have specific globular cluster frequencies ($S_{\rm N}$, number per unit luminosity) as high as those in giant elliptical galaxies (Harris 1991). Larger surveys of dEs in the Virgo and Fornax Clusters revealed a trend of increasing $S_{\rm N}$, or an increase in the scatter of $S_{\rm N}$, with decreasing galaxy luminosity (Durrell et al. 1996; Miller at al. 1998). This trend is consistent with a constant GC formation efficiency but decreasing field star formation efficiency because of supernovae feedback from the forming clusters. Miller at al. (1998) also showed that the mean $S_{\rm N}$ for nucleated dEs is

about double that for non-nucleated dEs. This has implications for the formation of nuclei and the progenitor galaxies of non-nucleated versus nucleated dEs. However, the sample size was still relatively small (24 dEs in Miller et al.'s HST sample) and the comparison with the GC systems of dIs was limited to dIs in the Local Group, which is a very different environment from the Virgo or Fornax Clusters. Therefore, the *HST* WFPC2 surveys were extended to include more dE galaxies and some dI galaxies in the Virgo and Fornax Clusters (Lotz et al. 2004; Seth et al. 2004). Also, a search for GCs in 57 dwarfs in nearby groups and in the field was carried out by Sharina et al. (2005) and the Virgo and Fornax Clusters have also been surveyed with ACS on HST (Côté et al. 2004; Jordán et al. 2007a). Finally the sample of galaxies with studied cluster systems is large enough to start making meaningful comparisons between different types of dwarfs in different environments.

These large samples are also needed for studying the globular cluster luminosity function (GCLF) in dEs. Each dwarf has only a few GCs, so samples from different galaxies must be combined into a composite GCLF (Durrell et al. 1996). Because dwarfs have lower density disks than galaxies like the Milky Way, the dominant processes that destroy GC will work more slowly in them. Therefore, the GCLF, more precisely the GC mass function, in dwarfs has presumably undergone less modification and is closer to the initial GC mass function than in the GC systems of giant spiral or elliptical galaxies. Any differences in the GC mass function must be explainable by theories of GC formation and destruction combined with hierarchical models of the merging of galaxies and the formation of GC systems (e.g. Beasley et al. 2002; Kravtsov & Gnedin 2005).

Therefore, in this paper we present an analysis of the GCLF and specific luminosities and masses for the full 69 galaxy sample from the *HST* WFPC2 Dwarf Elliptical Snapshot Survey (Miller at al. 1998; Stiavelli et al. 2001; Lotz et al. 2001, 2004). The observations are summarized in Section 2 and the new analysis and results are given in Section 3 and discussed in Section 4. Throughout the work use the *HST* Cepheid Key Project (Freedman et al. 2001) distances to the galaxy clusters: $(m-M)_0$(Leo) = 30.0; $(m-M)_0$(Virgo) = 30.92; $(m-M)_0$(Fornax) = 31.39.

2. Observations

Imaging of the 69 dE galaxies in the *HST* Dwarf Elliptical Snapshot Survey was obtained with WFPC2 on the *Hubble Space Telescope* in Cycles 6, 7, and 9 (GO programs 6352, 7377, and 8500). The galaxies were selected from catalogs of the Virgo and Fornax Clusters (Binggeli et al. 1985; Ferguson 1989) and the Leo Group (Ferguson & Sandage 1990). The dE galaxies have absolute magnitudes in the range $-12 < M_B < -17$ and includes 45

nucleated galaxies and 24 non-nucleated galaxies. The images were taken with the F555W (2×230 sec) and F814W (300 sec) filters and the galaxies were centered on chip WF3 to maximize the spatial coverage. More details about the final data reduction, the selection of the GC candidates, and the photometry can be found in Lotz et al. (2004).

The global properties of the sample galaxies and the net number of GC candidates per galaxy are given in Tables 1 and 2 for nucleated and non-nucleated galaxies, respectively. To quickly summarize Lotz et al. (2004), the GC candidates are selected to be compact ($\mathrm{FHWM_{F555W}} < 2.5$ pixels) and to have colors typical of GCs ($0.5 < V - I < 1.5$ with $\sigma(V - I) < 0.3$). "Object+background" candidates are those within 5 scale lengths of the centers of the galaxies while "background" candidates are those detected outside of 5 scale lengths. The net number of GC candidates in a galaxy, N_{GC}, is then the number of "object+background" candidates minus the number of "background" candidates scaled to the area within 5 scale lengths.

These values of N_{GC} do include the nuclei. This is justified for the fainter nuclei since their properties are essentially indistinguishable from bright GCs (Lotz et al. 2004). The brighter nuclei may form from mergers of GCs or star formation on top of an existing central GC (see Sec. 4 and Bekki, Couch, & Shioya 2006). Therefore, it is reasonable to count a bright nucleus as at least one GC. It should be noted that the subtraction of the bright GCs, or even all nuclei, from N_{GC} does not qualitatively change the results of this paper.

The values of N_{GC} in Tables 1 and 2 should be the same as those in Tables 2 and 3 of Lotz et al. (2004). However, we have found some sorting errors in the last column of Tables 2 and 3 of that paper have been corrected in the current tables. Only column N_{GC} of the tables in Lotz et al. (2004) has sorting errors and this does not affect any results in that paper.

3. Results

3.1. Globular Cluster Luminosity Function

As can been seen from Tables 1 and 2, the typical galaxy in our sample has about 6 GC candidates and the maximum number in any one galaxy is 52 in VCC 940. Therefore, no single galaxy has enough clusters to yield an accurate luminosity function. Therefore, as is common practice in these types of analyzes, we must combine the GC candidates from many galaxies to derive a mean dE GC luminosity function (GCLF). In this case, we derive the GCLF for the galaxies in the Virgo and Fornax Clusters separately since all the galaxies in each cluster are at approximately the same distance. Obtaining the net GCLF requires

correction for foreground/background objects and the photometric completeness function.

Subtracting the foreground and background contamination is similar to what is done to determine $N_{\rm GC}$, but now all GC candidates for a given galaxy cluster are considered as an ensemble. The total sample of "object" candidates is a merged list of all the object candidates (within 5 scale lengths). Likewise, the total sample of "background" candidates includes all candidates classified previously as background. The background LF is then scaled by the ratio of the total areas used for selecting the "object" and "background" candidates.

The completeness curve is derived using standard artificial "cluster" tests. The object PSFs used for the tests are the sum of several bright GC candidates taken from the WF3 image of VCC 1254. Artificial GCs of different magnitudes are then added to representative WFPC2 images using the DAOPHOT task ADDSTAR in IRAF[3]. During each trial the number of artificial objects added is only 20% of the number of actual objects found in a given magnitude bin so that the artificial objects do not affect the crowding in the image. Hundreds of trials are run in order to build up adequate statistics. The same object detection algorithm used to select the actual candidates is then used to detect the artificial GCs and the ratio of the objects found to the objects added gives the completeness fraction. The completeness function is then characterized by Pritchet's interpolation function (Fleming et al. 1995). The completeness functions for the Virgo and Fornax samples are shown in Figure 1. The limiting magnitudes, where the completeness fraction drops to 0.5, are $V_{lim} \approx 25$ and $I_{lim} \approx 24$ but differ slightly between Virgo and Fornax Cluster images. This may be due to small changes in the mean sky background.

The background subtraction and fitting of the GCLFs are done using the method of Secker & Harris (1993). The best-fitting parameters of either a Gaussian or a t_5 distribution are found using a maximum-likelihood technique which avoids binning the data and takes into account the completeness function and the photometric error as a function of magnitude. The quoted mean parameter values and their errors are from one-dimensional projections of the two-dimensional maximum-likelihood distribution. As found by Secker (1992) and Secker & Harris (1993), the t_5 distribution,

$$\gamma(m) = \frac{8}{3\sqrt{5}\pi\sigma_t}\left[1 + \frac{(m-m^0)^2}{5\sigma_t^2}\right]^{-3}, \qquad (1)$$

gives a better fit than a Gaussian distribution because the power-law form of the wings

[3]IRAF is distributed by the National Optical Astronomy Observatories, which are operated by the Association of Universities for Research in Astronomy, Inc., under cooperative agreement with the National Science Foundation.

of the t_5 distribution matches the GCLF better than the exponential form of a Gaussian. Therefore, we only quote the results of the t_5 fits.

Lotz et al. (2004) showed that the integrated properties of dE GC candidates and dE nuclei are very similar. Photometrically nuclei are like bright, somewhat red, globular clusters. Therefore, we first calculate the GCLF of GC candidates and nuclei together. The GCLFs are given in Tables 3, 4, and 5 and are shown in Figures 2 and 3. The parameters of the best fits are given in Table 6. The parameters for the candidates in the Virgo Cluster are much more accurate than the parameters from the Fornax Cluster because the Virgo Cluster is 0.5 mag closer than Fornax, so clusters are detected further down the GCLF, and because the Virgo sample is larger. Both the absolute peak magnitudes and the widths are the same within the errors with mean values of $M_V^0 \approx -7.3 \pm 0.1$ and $M_I^0 \approx -8.1 \pm 0.1$ and $\sigma_{t,} \approx 1.0 \pm 0.1$ mag. In theory the equivalent Gaussian width is $\sigma_G = 1.29\sigma_t \approx 1.3$ mag. However, in practice the widths from Gaussian fits are narrower than the theory would predict. A Gaussian fit to the Virgo GC+nuclei sample gives $m_V^0 = 23.61 \pm 0.13$ with $\sigma_G = 1.16 \pm 0.15$. This is consistent with the t_5 fit and narrower than expected analytically.

It is also of interest to look at the luminosity functions of the GC candidates without the nuclei and of the nuclei themselves. The GCLF parameters for the GC sample that excludes the nuclei are given in Table 6 and they are the same, within the errors, to the sample with GCs plus nuclei. Figure 4 shows the luminosity function of the nuclei themselves. For this fit the magnitudes of the nuclei in the Fornax galaxies have been adjusted to the distance of the Virgo Cluster. The LF of the nuclei is peaked with $M_V^0 \approx -9.7$ (Table 6).

In the Virgo Cluster there are a sufficient number of galaxies that we can also look for differences in the GCLF between nucleated and non-nucleated galaxies. The GCLF for dE,N galaxies, excluding the nuclei, gives $m_V^0 = 23.69 \pm 0.11$ (Table 6). Including the nuclei gives an indistinguishable result of $m_V^0 = 23.66 \pm 0.13$. Not surprisingly given that the majority of the total sample of Virgo GCs come from dE,N, the GCLF peak for the dE,N galaxies of $M_V^0 = -7.23 \pm 0.11$ is similar to the result for the full sample (Table 6). The peak magnitude for the dE,noN galaxies is $M_V^0 = -7.50 \pm 0.17$, 0.2 magnitudes brighter than that of the dE,N galaxies, but this difference has a significance of only 1.2 sigma. Therefore, V-band the GCLFs in dE,Ns and dE,noNs are the same within the uncertainties.

Thus far we have assumed that all the galaxies in sample are at the mean distances of their respective groups or clusters. However, each of these physical structures has some depth, recent distance measurements of galaxies in the Virgo Cluster have shown that it has a line-of-site depth of between 3 and 4 Mpc (Jerjen et al. 2004; Jordán et al. 2005). Therefore, we have run Monte-Carlo simulations of composite GCLFs drawn from 69 galaxies drawn from Gaussian distance distributions with a mean of 15.3 Mpc and sigma parameters between

1 Mpc and 4 Mpc. The distribution of galaxy absolute magnitudes is the same as for the actual sample. The number of simulated clusters per galaxy is derived from a fit to $N_{\rm GC}$(tot) vs. M_B, modulated for Poisson statistics The distribution of simulated GC brightness comes from a t_5 distribution with $M_V^0 = -7.3$ and $\sigma_t = 1.1$ at our assumed distance of the Virgo Cluster. The parameters of the combined GCLFs were measured with the same procedure used for the real data. The results of the simulations are shown in Table 7. As the line-of-sight distribution of galaxies increases the measured peak becomes systematically brighter and broader than the actual distribution. However, as long as the sigma of the galaxy distribution is less than 2 Mpc (corresponding to a line-of-sight FWHM of 4.7 Mpc), the systematic errors are not significant. Also, none of the galaxies in our sample are members of substructures such as the W, W′, or M clouds that are more distant than the main Virgo Cluster. Therefore, we conclude that our results for M_V^0 and σ_t are not significantly biased by the finite depths of the Virgo and Fornax Clusters.

A log-normal or Gaussian luminosity distribution per unit magnitude can also be described by a broken power-law when converted to number per unit luminosity (Harris & Pudritz 1994). Figure 5a shows the background-subtracted luminosity function $\log(\phi(L)/L)$ versus log luminosity for GCs and nuclei in the Virgo sub-sample. The best-fitting t_5 function from Figure 2 is plotted with the dashed line. Above $\log(L/L_\odot) \approx 5$ the GCLF is well-fit with a power-law with slope $\alpha = -1.9 \pm 0.1$ (straight black line). The result is the same if the nuclei are excluded. This slope is consistent with the bright-end GCLF slopes for young star clusters (e.g. Whitmore et al. 1999) and old GCs in spiral and elliptical galaxies (Harris & Pudritz 1994).

Recently van den Bergh (2006) claimed that the break in the power-law GCLF is present only for galaxies brighter than $M_V = -16$ but that the GCLF for fainter galaxies is an unbroken power-law. Figure 5b shows the GCLF (GC + nuclei) for Virgo galaxies with $M_V > -15.75$ and the values are given in Table 8. The limit of $M_V = -15.75$ was chosen because there is a natural break in the distribution of M_V for the WFPC2 sample at this value. The best-fitting power-law has a slope $\alpha = -1.7 \pm 0.2$ (solid line), consistent with that for the full sample. Because of the smaller sample size there is less evidence for a break in the power-law. The best-fitting t_5 function (dash-dot line) has a brighter peak and a much broader σ_t than the best fit for the full sample. However, the standard fit for the full sample (dashed line) is still a reasonable match to the data. Deeper data and a bigger sample are needed to confirm whether the GCLF for faint galaxies in the Virgo Cluster is different from the GCLF for the brighter galaxies.

3.2. Specific Frequency

Specific globular cluster frequency, $S_{\rm N}$, is defined as the number of globular clusters per unit V-band luminosity, normalized at $M_V = -15$:

$$S_{\rm N} = N_{\rm GC}({\rm tot})10^{0.4(M_V+15)} \quad (2)$$

where $N_{\rm GC}({\rm tot})$ is the total number of globular clusters (Harris & van den Bergh 1981). With the completeness function and luminosity function known we can correct $N_{\rm GC}$ for the undetected portion of the GCLF and then calculate $S_{\rm N}$. The completeness corrections are determined by dividing the integrals of the measured GCLFs alone by the integrals of the GCLFs multiplied by the completeness functions. These factors are 1.04, 1.17, and 1.24 for Leo, Virgo, and Fornax, respectively. For the galaxy absolute magnitude we use $M_V = M_B - 0.77$, where 0.77 is the mean $B-V$ color for the dE galaxies in the study of van Zee et al. (2004). The *HST* data itself cannot be used to determine the total V magnitude in all cases since the signal-to-noise for many of the fainter galaxies is not enough to give a reliable magnitude.

The computed values for $N_{\rm GC}({\rm tot})$ and $S_{\rm N}$ are given in Tables 9 and 10 and plotted in Figure 6. The overall trends noticed by Miller at al. (1998) in a subset of the current data are still apparent, $S_{\rm N}$ increases with increasing M_V (decreasing luminosity). Also, on average nucleated galaxies have higher $S_{\rm N}$ than non-nucleated galaxies: $\bar{S}_{\rm N}({\rm dE,N}) = 8.7 \pm 1.6$ and $\bar{S}_{\rm N}({\rm dE,noN}) = 4.3 \pm 1.1$ where the uncertainties are the standard deviations of the mean. These values are slightly higher than the values in Miller at al. (1998) since the current, larger sample contains more faint galaxies which typically have higher values of $S_{\rm N}$.

Since $S_{\rm N}$ is correlated with galaxy absolute magnitude, it is also correlation with any other property that depends on the galaxy brightness. For example, it is well known that the surface brightness profiles of faint dEs have Sersic exponents near 1 (exponential) while brighter dEs are more cuspy with exponents approaching 4, equivalent to an $R^{1/4}$ profile (Graham & Guzman 2003). Put another way, more luminous dEs have higher surface brightnesses. Figure 7 shows how the scatter in $S_{\rm N}$ increases with decreasing central surface brightness for the sub-sample of the current sample in Stiavelli et al. (2001). The mean central surface brightness from Sersic fits for 14 dE,N galaxies is $\mu_0(V) = 21.3 \pm 1.6$ while for 10 dE,noN galaxies it is about 1 magnitude fainter, $\mu_0(V) = 22.2 \pm 1.5$.

There is also an environmental dependence on $S_{\rm N}$ in the sense that the number density of dE,N galaxies is more centrally concentrated than that of the bright dE,noN galaxies in the Virgo and Fornax Clusters (Ferguson & Sandage 1989). However, there is no direct radial dependence on $S_{\rm N}$ with projected radial position within the Virgo Cluster or with projected radial distance from the nearest bright ($M_B < -18.6$) galaxy (Figure 8).

3.3. Globular Cluster T Parameter and Mass Fractions

$S_{\rm N}$ is a very useful quantity since it is dependent only on basic measurements and it has a long history in the literature for comparison. However, because it is based on a luminosity it is applicable only to old stellar systems with similar mass-to-light (M/L) ratios. It is important to be able to compare the star cluster systems in different types of galaxies, so a quantity like $S_{\rm N}$ is needed that is independent of M/L. Such a parameter is the T parameter of Zepf & Ashman (1993),

$$T = \frac{N_{\rm GC}({\rm tot})}{M_G/10^9 M_\odot} \tag{3}$$

where $N_{\rm GC}({\rm tot})$ is the total number of clusters and M_G is the stellar mass of the galaxy. M/L values are not available for each galaxy so we have adopted $M/L_V = 5$, a typical value for dE galaxies from the spectroscopic measurements of Geha et al. (2002). Values of $T(V)$ for the current sample are given in Tables 9 and 10. Not surprisingly, Figure 9 shows that $T(V)$ exhibits the same trends with galaxy mass as $S_{\rm N}$ has with M_V. Likewise, the mean $T(V)$ for the nucleated galaxies is about a factor of two higher than the mean for the non-nucleated galaxies: $\bar{T}({\rm dE,N}) = 20.4 \pm 3.9$ and $\bar{T}({\rm dE,noN}) = 10.2 \pm 2.6$.

Finally, it is of interest to estimate the mass fraction of the stellar light currently in star clusters. Because of the uncertainties in estimating the total mass in GCs in any galaxy given the small number statistics, we calculate the mass in two ways and average the results. In both cases we assume $M/L_V = 2$ for each GC. The "specific mass", or percentage of stellar mass in GCs is

$$F = 100\frac{M_{GC}}{M_G}. \tag{4}$$

In the first method we take advantage of the fact that we believe that we know the form of the mass function. The total mass of clusters should then be roughly equal to the mean cluster mass times the number of clusters. Integrating over $M\phi(M)$, $\phi(M) = \phi(L) * M/L_V$ where $\phi(L)$ is the t_5 function shown in Figure 5a and we assume $M/L_V = 2$, gives a mean mass of $M = 4.3 \times 10^5\ M_\odot$. The mass fraction then is given by $F = 0.0433T$.

In the second method, the magnitude of each object in the "object+background" sample is converted to a mass assuming $M/L_V = 2$. Second, from the total (GC + background) and background luminosity functions we compute a probability that an object of a given magnitude is an actual GC rather than a background object,

$$P(V) = 1 - \frac{\phi_{bkg}(V)}{\phi_{tot}(V)}. \tag{5}$$

For example, in Figure 2 the $\phi_{tot}(V)$ are the thick solid curves (normalized column 2 of Tables 3 and 4) and the $\phi_{bkg}(V)$ are the dotted curves (column 3 of Tables 3 and 4). A

fourth order polynomial is fit to $P(V)$ in order to smooth it and the results for the Virgo and Fornax samples are shown in Figure 10. The total mass of clusters for each galaxy is then the sum of the cluster masses times the probability that each is an actual cluster. No additional correction is made for the unobserved portions of the GCLFs, but this should be a small factor since most of the mass is in the most massive clusters.

The two methods give results that are consistent within about a factor of two. The mean values of $F(V)$ from these two methods and their uncertainties are also in Tables 9 and 10. The trends in $F(V)$ with galaxy mass are similar to those seen with the other parameters (see Figure 11) and the mean values are $\bar{F}(\mathrm{dE,N}) = 0.9 \pm 0.2$ and $\bar{F}(\mathrm{dE,noN}) = 0.7 \pm 0.3$. The mean for the non-nucleated dwarfs is biased by one outlying point, VCC 1781 with $F = 7.5 \pm 7.8$. Removing this point gives $\bar{F}(\mathrm{dE,noN}) = 0.5 \pm 0.1$.

4. Discussion

4.1. Globular Cluster Luminosity Functions

An important question is whether the globular cluster luminosity and mass functions in dwarf galaxies are the same as those in spiral or giant ellipticals. The comparison will have implications for theories of globular cluster formation and evolution and will put constraints on the fraction of globular clusters in different types of giant galaxies that were formed in dwarf galaxies and later accreted. First we compare our results on the form of the GCLF and GC mass function in dEs with previous authors and then address the issue of how the GCLF of dEs compares with other types of galaxies.

Our best measurement of the shape of the GCLF comes from the Virgo sample. The V-band GCLF for the Virgo dEs is well-fit by a t_5 or Gaussian function with $M_V^0 = -7.3 \pm 0.1$ and $\sigma_t = 1.0 \pm 0.1$ mag (as mentioned above, a Gaussian fit give $\sigma_G = 1.2 \pm 0.2$). Durrell et al. (1996) measured the GCLF peak from a sample of 11 Virgo dEs to be $T1^0 = 23.6 \pm 0.3$. With $(V - T1) = 0.5$ and using our adopted distance modulus of 30.92 for Virgo, this gives $M_V^0 = -6.8 \pm 0.3$ which is not consistent with our results. Sharina et al. (2005) have recently studied the GC systems of a sample of dwarfs with distances between 2 and 6 Mpc with *HST*. The GCLF for the dEs has a peak at $M_V^0 \approx -7.4$ but at $M_V > -6$ the numbers continue to rise instead of decrease. Our data do not go deep enough to investigate the shape of the faint end of the GCLF. Also, Beasley et al. (2006) have studied the system of ~ 77 GCs in the Virgo dE VCC 1087 and found that $g^0 = 24.1 \pm 0.3$. With $V \approx g - 0.3$ (Bruzual & Charlot 2003), this gives $M_V^0 = -7.1$ for $(m - M)_0 = 30.92$ (mean Virgo distance modulus) or $M_V^0 = -7.5$ for $(m - M)_0 = 31.27 \pm 0.14$ (Jerjen et al. 2004, SBF distance). Therefore,

this result is consistent with ours within the uncertainties in the peak measurement and the distance.

In the I-band we find $M_I^0 = -8.1 \pm 0.1$ for the Virgo Cluster dE "GC + nuclei" GCLF and $M_I^0 = -8.0 \pm 0.4$ for the Fornax Cluster dE "GC + nuclei" GCLF. These values are fainter than the GCLF turnover luminosity for giant ellipticals, $M_I^0 = -8.46 \pm 0.03$, found by Kundu & Whitmore (2001).

The literature to date has been somewhat undecided about whether the GCLF of dE differs from that of giant ellipticals. Figure 2 of the review of (Harris 1991), which includes only the four Local Group dEs with GCs known at the time, shows a small but statistically insignificant trend that the GCLF peak in dwarfs may be fainter than in giants. Based on the statistics available Harris concluded that the GCLF peak is fairly independent of galaxy mass. Durrell et al. (1996) found that the the peak from their dE sample was 0.4 mag fainter than the GCLF peak of M87 from Whitmore et al. (1995). Note that Durrell's GCLF peak is about 0.5 mag fainter than is currently found. Strader et al. (2006) claim that a comparison of GCLF peaks in dEs and gEs in Virgo are consistent. However, Jordán et al. (2006, 2007b), using the same ACS Virgo Survey dataset, find that the GCLF peak magnitudes tend to scatter towards fainter values in lower-luminosity galaxies.

Recently Di Criscienzo et al. (2006) have done a systematic analysis of the literature to determine if there are differences in the GCLF peaks between the GC systems of the Galaxy, M31, and giant ellipticals. All distances were put on a consistent scale calibrated to RR Lyraes and Cepheids assuming that $\mu_0(LMC) = 18.50$. Similar selection criteria are used for the Milky Way and M31 samples. Metallicity corrections to the Cepheid distances to the galaxies used to calibrate the surface brightness fluctuation (SBF) method are from theoretical models rather than the empirical relation used by the *HST* Key Project. This gives better agreement between the Cepheid and SBF distances. Finally, metallicity corrections from Ashman et al. (1995) are applied to the GCLF peak magnitudes so that all peaks are for [Fe/H] $= -1.6$. The result is that the GCLF peaks the metal-poor GC populations are very constant with $M_{V,Z}^0(MW) = -7.66 \pm 0.11$, $M_{V,Z}^0(M31) = -7.65 \pm 0.19$, and $M_{V,Z}^0(gE) = -7.67 \pm 0.23$. For comparison with the current work, using the Cepheid calibration from Freedman et al. (2001) gives $M_{V,Z}^0(gE) = -7.83 \pm 0.23$.

From Lotz et al. (2004) the mean GC color is $\langle V - I \rangle = 0.90$. According to the following color-metallicity relation from Kissler-Patig et al. (1998)

$$[\mathrm{Fe/H}] = -4.5 + 3.27(V - I) \tag{6}$$

the mean metallicity of the dE GCs is [Fe/H] $= -1.6$. This is the same as the metallicity of the metal-poor GC samples from Di Criscienzo et al. (2006), so no additional metallicity

correction to the dE GCLF peak is needed and $M^0_{V,Z}(dE, HST) = -7.3 \pm 0.1$

A comparison of the GCLF peak results is shown in Figure 12. Except for the three filled circles all of the values have been adjusted, where appropriate, to use the HST Key Project distance moduli used in this paper. The three filled circles use Di Criscienzo et al.'s preferred distance scale which implies a Virgo distance modulus of $(m - M)_0 = 30.76$. In general, the peak GCLF magnitudes for the dEs are fainter than the peak magnitudes for the MW, M31, and gEs, though the statistical significance in each individual result is only 1–1.5 sigma. The indication from all the results together is that the GCLF peak in dEs is similar to or fainter by ~ 0.5 magnitudes than the peak in giant galaxies. That our I-band peak magnitudes are also ~ 0.4 mag fainter than those measured in giant ellipticals adds support to this result.

The shapes and peaks of the observed GCLFs in different types of galaxies are important for what they reveal about the underlying GC mass function (GCMF). As shown in Figure 5, peaks in the GCLF as plotted as number per unit magnitude become bends or flattenings when plotted as number per unit luminosity or mass. Assuming $M/L = 2$, then $M^0_{V,Z}(dE, HST) = -7.3 \pm 0.1$ corresponds to $\log(m^0(dE, HST)) = 5.15 \pm 0.04$ while $M^0_{V,Z}(gE) = -7.66 \pm 0.11$ gives $\log(m^0(gE)) = 5.29 \pm 0.05$. The bright-end slope of these luminosity or mass functions is consistent with a power-law $N(L) \propto L^\alpha dL$. In the Milky Way, M31, and gEs α is typically between -1.6 and -2 (e.g. Harris & Pudritz 1994; McLaughlin 1994; Larsen et al. 2001). Very young star clusters in merging and starburst galaxies also have nearly pure power-law luminosity functions with α between -1.8 and -2 (e.g. Miller et al. 1997; Whitmore et al. 1999; Goudfrooij et al. 2004). The bright-end slope of the GCLF for the entire Virgo dE sample (Figure 5a) is -1.9 ± 0.1, consistent with with previous results for dEs (Durrell et al. 1996) and with the bright end slopes in the Milky Way and M31 and young cluster systems. This slope is somewhat steeper than the bright-end slopes found in many gEs (see Harris & Pudritz 1994).

Some interesting results from the Virgo ACS survey are that the peak GCLF magnitudes, or power-law break masses, and the width of the Gaussian distribution of magnitudes decrease with decreasing galaxy luminosity (Jordán et al. 2007b). As shown in Figure 12, the GCLF peak magnitude measured from the WFPC2 data agrees with the ACS value once the two results are put on the same distance scale and corrected for bandpass. The equivalent Gaussian width from the WFPC2 data is $\sigma_G = 1.16 \pm 0.15$. For galaxies with $-18 < M_B < -16$ the ACS result is $\sigma_G \approx 0.9 \pm 0.1$. The WFPC2 GCLF width is systematically higher than the ACS result at the 1.5σ level. This is also reflected in the fact that the bright-end power-law slope of $\alpha = -1.9 \pm 0.1$ is consistent with but on average shallower than the slopes measured for dwarf galaxies in the ACS sample.

The WFPC2 survey contains galaxies fainter than in the ACS Virgo survey so we can explore if the trends in peak magnitude and Gaussian sigma continue. The formal t_5 fit to the faint WFPC2 galaxy subsample gives a much brighter and broader GCLF than for the bright subsample. However, as can be seen in Figure 5b, this is not a reliable result. Due to the small number of GCs the GCLF peak for the fainter galaxies is consistent with the peak for the brighter galaxies. The width of the distribution for the faint galaxies is broader, if anything, than the width for the bright galaxies and the power-law slope is shallower. This is opposite to the trend suggested by the ACS results. Unfortunately, the number of GCs in the faint galaxies is too low to determine if this difference is significant.

Theoretically it is also not certain whether a trend of GCLF peak, or mass function turnover, with host galaxy mass is expected. The similarities between the bright end of the GCLF for old, metal-poor clusters and the power-law mass functions of young star clusters and giant molecular clouds has led to the idea that star clusters form with an initial power-law mass function which evolves with time as low-mass clusters are destroyed (Harris & Pudritz 1994; Gnedin & Ostriker 1997). Fall & Zhang (2001) show that if $M_{gal} \propto V_c^3$ then the mass function is independent of V_c while if $M_{gal} \propto V_c^4$ then the peak mass becomes *larger* for smaller V_c. However, Vesperini & Zepf (2003) find that the mean cluster mass of evolved populations does increase with host galaxy mass in rough agreement with the peak masses given above if the cutoff in the stellar IMF is $m_T = 0.9\ M_\odot$. One difference between the two works is that Vesperini & Zepf (2003) give their simulated clusters King model concentration indices that scale with cluster mass. However, all of the model host galaxies have $\log(M_{gal}) > 10.5$ and so are not true dwarfs. Earlier simulations with dwarf galaxy-sized objects predict mean cluster masses smaller than given by the current observations (Vesperini 2000, 2001). New simulations for dwarf-galaxy size hosts would be very useful.

4.2. Specific Frequencies and Mass Fractions

The high average $S_{\rm N}$ the trend of increasing $S_{\rm N}$ with decreasing galaxy luminosity, and the factor-of-two difference in $S_{\rm N}$ between nucleated and non-nucleated dwarfs all confirm the results of Miller at al. (1998) using the first 24 galaxies observed for the *HST* dE Snapshot Survey. Further, a Kolmogorov-Smirnov test comparing the distributions of $S_{\rm N}$ in nucleated and non-nucleated galaxies gives that the probability that they are drawn from the same distribution is only 3% (see below). There do seem to be systematically more GCs per unit luminosity in dE,N than in dE,noN galaxies not accounted for by the presence of nuclear star clusters alone.

One evolutionary pathway for dEs is the stripping of gas from dIs as they encounter

the dense intercluster medium in rich galaxy clusters. An important way of evaluating the importance of this mechanism is to compare the GC populations of dIs and dEs. New studies of the star clusters in dIs now allow us to make comparisons using roughly equal numbers of galaxies (Seth et al. 2004; Sharina et al. 2005). However, because dIs and dEs have different M/L ratios, the luminosity-based $S_{\rm N}$ is not the appropriate quantity to use for the comparison. Instead, we correct for M/L by calculating the T parameter for metal-poor GC populations, $T_{\rm MP}$, to compare the relative numbers of GCs in dIs, dEs, spirals and giant ellipticals. In this case we are only comparing the number of old (age $\gtrsim$ 10 Gyr), metal-poor ([Fe/H] $\lesssim -1$) clusters. We are assuming that all dE GCs are old and metal-poor. From the sample of Fornax and Virgo Cluster dIs from Seth et al. (2004) we use N_{red}, the number of cluster candidates with $V-I > 0.85$. Background subtraction and completeness corrections are done in the same way as described in that paper. The galaxies' absolute magnitudes are from their Table 1. We also include the 11 Virgo dEs and NGC 3115D1 whose clusters were identified by Durrell et al. (1996) and VCC 1087 (Beasley et al. 2006). When calculating the luminosities of these galaxies we use the distance moduli assumed throughout this paper. Sharina et al. (2005) identified GCs in *HST* snapshots of 57 dwarf galaxies with distances between 2 and 6 Mpc. From their Table 2 we select only those star cluster candidates with $0.7 < V-I < 1.5$ in order to exclude the bluest clusters in dIs. Finally, we include dwarf galaxies in the Local Group with old, metal-poor GCs (e.g. Da Costa & Mould 1988; Mateo 1998). To convert from galaxy luminosity to stellar mass we adopt $M/L_V = 5$ for all dE/dSph galaxies and $M/L_V = 2$ for all dI galaxies. To bridge the mass gap between dwarf and giant elliptical galaxies and we calculate $T_{\rm MP}$ for the *HST* ACS Virgo Cluster sample of 100 early-type galaxies (Côté et al. 2004; Peng et al. 2006). The number of metal-poor clusters is $(1-f_{red})N_{GC}$ from Table 2 of Peng et al. (2006). Galaxy masses are calculated from B_T given in Côté et al. (2004). As with the other dwarfs, we assume $(B-V) = 0.77$ and $M/L_V = 5$. Since the brightest galaxies in the ACS sample are much larger than the ACS field-of-view, the number of GCs given in Peng et al. (2006) will give systematically low values of $T_{\rm MP}$ without additional corrections. Therefore, we plot only galaxies with $B_T > 11$ ($M_V > -20.7$). Also, for galaxies with $M_V < -19.5$ we multiply the number of GCs by 1.5 to roughly correct for the fact that the spatial extent of these GCS is somewhat larger than the ACS field. The final corrected numbers of GCs for the ACS sample are being computed by the ACS Virgo team (Jordán et al. 2006). Finally, for a comparison with spiral and giant elliptical galaxies we use the values of $T_{\rm MP}$ from Goudfrooij et al. (2003), Chandar et al. (2004), and Rhode et al. (2005).

Figure 13 shows how $T_{\rm MP}$ depends on galaxy stellar mass. On the right axis we also show the equivalent mass fraction of GCs, $F_{\rm MP}$, assuming a universal GCLF so that $F_{\rm MP} = 0.0433 T_{\rm MP}$ (see above). It is notable that there is a single trend of $T_{\rm MP}$ that is obeyed by

all types of galaxies over 6 orders of magnitude of galaxy mass. The lower limit to the distribution is the line of $N_{\rm GC} = 1$ (dotted line). A few points fall below this line because the statistical background subtraction of the *HST* survey can result in the net number of GCs being less than one. There also appears to be an upper envelope to the values of $T_{\rm MP}$ that is a line from the points for the faintest dwarfs through the points for the most massive ellipticals. The equation of this line is

$$\log(T_{\rm MP}) = 5.4 - 0.4\log(M/M_{\odot}). \quad (7)$$

Table 11 gives the mean values of $S_{\rm N}$ $T_{\rm MP}$, and $F_{\rm MP}$ for different galaxy samples. For the dwarfs the statistics are computed for galaxies with $7.5 < \log(M/M_{\odot}) < 10$ to avoid biasing the results from the literature samples upward. These statistics do not include the Virgo ACS sample because of the many uncertain corrections that are needed to $N_{\rm GC}$. The mean properties from the *HST* dE snapshot survey agree well with the values for dEs from the literature. The importance of correcting for galaxy M/L using T is also seen for the dIs. The mean $S_{\rm N}$ for the dIs is about a factor of 3 lower than the mean $S_{\rm N}$ for the dEs. However, the mean $T_{\rm MP}$ and $F_{\rm MP}$ for the dIs is comparable to that for the dEs, especially dE,noNs. Giant galaxies have much smaller values of mean $T_{\rm MP}$ and $F_{\rm MP}$ than in dwarfs. As shown in previous studies, giant cluster ellipticals do have somewhat larger values of $T_{\rm MP}$ than field ellipticals or spirals (Rhode et al. 2005).

However, the comparison between different samples of dEs and dIs is complicated since the sample of dI galaxies in rich clusters that have been surveyed for GCs is still very small and it is biased towards more massive galaxies. Also, comparing mean properties is problematic given the increase in dispersion with diminishing mass.

Therefore, we have also run two-side Kolmogorov-Smirnov tests to compare the cumulative distributions of $T_{\rm MP}$ for different samples (Table 12). In Table 12 a N, HST, or noN designation refers to the *HST* Snapshot Survey, "Lit" denotes data taken from the literature, G is for galaxies in groups or the field, "C" is for galaxies in the Virgo or Fornax Clusters. As before, we have not included the ACS Virgo galaxies in the statistics. This shows that $T_{\rm MP}$ from the *HST* Snapshot Survey and from the literature are consistent with each other. However, the distribution of $T_{\rm MP}$ in dE,N and dE,noN galaxies are not consistent with being drawn from the same distribution. At low masses $T_{\rm MP}$ for dE,noN and dI galaxies are very similar but the probabilities diminish somewhat for higher galaxy masses. The distribution of $T_{\rm MP}$ for dE,N galaxies is similar to that for the small sample of dI galaxies in clusters, but not to that of dIs in groups.

Now we are in a position to try to understand these trends. That giant elliptical galaxies have higher $S_{\rm N}$ or $T_{\rm MP}$ than spirals can be explained by hierarchical merging (see Rhode et

al. 2005; Bekki, Yahagi, & Forbes 2006). Kravtsov & Gnedin (2005) have run cosmological N-body simulations of the formation of galaxies with halo masses greater than 10^{10} $M_{\odot}$ and found a correlation on GC mass fraction with halo mass. Their prediction of the baryonic mass fraction of GCs is the solid line in Figure 13. This prediction agrees with with the measured values of $F_{\rm MP}$ for spiral and massive ellipticals. This trend results from a relatively constant fraction of halo mass being turned into GCs (also see McLaughlin (1999)).

The trend of increasing $T_{\rm MP}$ or $F_{\rm MP}$ seen below $\log(M/M_{\odot}) \approx 10.5$ is thought to exist because lower mass halos are more susceptible to losing gas via supernovae and stellar winds generated by the formation of massive clusters. This will reduce the average star formation rate in lower-mass dwarfs and increase the relative fraction of mass in massive star clusters, thus increasing $T_{\rm MP}$. McLaughlin (1999) used the SNe wind models of Dekel & Silk (1986) to reproduce the trends in $S_{\rm N}$ seen by Durrell et al. (1996) and Miller at al. (1998). In this CDM-based model $T_{\rm MP} \propto M^{-0.4}$ and the two dashed lines in Figure 13 show this trend with two normalizations. The upper line is Equation 7 and defines the upper envelope of the $T_{\rm MP}$ trend. The other line is $\log(T_{\rm MP}) = 4.645 - 0.4\log(M/M_{\odot})$ and is the prediction of Equation 27 from McLaughlin (1999) for $M/L_{V,GC} = 2$, $M/L_{V,Gal} = 5$, and a GC formation efficiency of 0.26%. This confirms that this model is a good representation of the data.

Recently Forbes (2005) discussed the trend of increasing $S_{\rm N}$ with decreasing mass using only the ACS Virgo data. The increase in $S_{\rm N}$ for $\log(M/M_{\odot}) < 10.5$ is compared to new feedback models of Dekel & Birnboim (2004) which predict that $M/L_V \propto M^{-2/3}$ or $L_V \propto M^{5/3}$. As shown by Forbes (2005), $S_{\rm N} \propto M^{-5/3}$ is a reasonable match to the ACS Virgo data assuming that $N_{\rm GC}$ is constant. However, $N_{\rm GC}$ is not constant with galaxy mass and a slope this steep is does not match the trends of $S_{\rm N}$ or $F(V)$ when all the galaxies from the current analysis are considered. However, it can be shown that the prediction of Dekel & Birnboim (2004) that $M/L_V \propto M^{-2/3}$ is consistent with $M_{gas}^{init}/M_* \propto L_*^{-0.4}$ found by McLaughlin (1999) using the Dekel & Silk (1986) wind models. Therefore, the new wind models do appear to be consistent with the previous calculations and with the data.

Bekki, Yahagi, & Forbes (2006) have recently run N-body cosmological simulations to investigate the origin of this trend. They find that the data for galaxies with $M_V < -16$ can be reproduced if $M/L_V \propto M^{-1}$ and if the formation of metal-poor GCs is truncated at $z = 15$ (presumably due to winds or reionization). The lower $S_{\rm N}$ or $T_{\rm MP}$ in higher-mass dwarfs is due to the merging of small halos, many of which do not have GCs since they virialized after $z = 15$. It would be interesting to compare the results of these simulations with the larger set of dwarf galaxy data presented here. Also, observational ages and total halo masses are needed to test the results of these simulations.

At a given mass there is considerable scatter in $T_{\rm MP}$, especially for the dwarfs, from 0 to

a value given approximately by Equation 7. At least some of this scatter should be due to intrinsic variations in properties and processes. In the model of McLaughlin (1999) variations in $T_{\rm MP}$ would be produced by variations in the GC formation efficiency, $\epsilon_{\rm cl} = M^{\rm init}_{\rm gcs}/M^{\rm init}_{\rm gas}$. Therefore, natural variations in the initial gas fraction and the details of the star formation and ISM-feedback processes will affect $T_{\rm MP}$. It is likely that stochastic effects become more important in lower-mass galaxies since single star formation events can have global impacts. Variations in M/L will also contribute to the scatter.

The differences between nucleated and non-nucleated dEs and the comparison with dEs and dIs in clusters and the field suggest shows that environmental effects are important. The similarities of the GCS properties between dE,noN galaxies in clusters and dI galaxies suggests that dE,noNs may be the result of dI galaxies that were simply stripped of gas when they fell into the cluster. However, in dE,N star and cluster formation occurred in addition to gas stripping. Bekki, Couch, & Shioya (2006) has shown that interactions can produce gas inflow and central star formation that can lead to nuclei. Therefore, it is likely that the progenitors of dE,N galaxies were those that experienced significant interactions, either because they were formed deeper in the potential well of the galaxy cluster or because of the particular characteristics of their orbits.

Virgo and Fornax represent different environments in that they have very different galaxy number densities, yet we don't see a significant difference in the dE GCLFs of the two clusters. Processes on a "local scale" that depend on the dwarf's location within a cluster can affect its star cluster formation history hence the difference between dE,N, dE,noN and dIs. But these processes are fairly similar in Virgo and Fornax (and don't strongly depend on the galaxy cluster mass or density) so we don't encounter a large difference between the two galaxy clusters.

Presumably the cumulative effect of "local" processes that affect star cluster formation (e.g. interactions, ram-pressure stripping) do depend on the galaxy cluster properties. For example, cluster velocity dispersion affects the nature of interactions and the efficiency of ram pressure stripping. Therefore, more massive clusters could have different dE to dI and dE,N to dE,noN ratios than less massive clusters. The similarities seen here between Virgo and Fornax may be due to the selection effect that we are only considering true dEs that have completed the transformation from dIs. Therefore, the star-formation histories of dEs in Virgo and Fornax are not that different. The GCLFs for a mass-selected dwarf galaxy population that includes more dI and transition objects may show some dependence on galaxy cluster properties.

Higher star formation rates will produce both new star clusters and field stars. To enhance $S_{\rm N}$ or $T_{\rm MP}$ the process must be biased in favor of star clusters. This would occur

if star cluster formation occurs first and the subsequent supernovae, perhaps aided by ram pressure stripping, truncates field star formation (McLaughlin 1999). This is plausible since star cluster formation probably occurs in the densest, most rapidly collapsing regions of gas. The field stars that are formed in the galaxies centers will produce the higher central surface brightnesses seen in luminous dE,N (see Figure 7). Luminous nuclei can then form via the merging of central GCs via dynamical friction (Hernandez & Gilmore 1998; Oh & Lin 2000; Bekki, Couch, & Shioya 2006; Miocchi et al. 2006). Because the star formation occurs over an extended period, especially in the more massive galaxies, this will lead to massive nuclei which are redder, younger, and more metal-rich than the typical GC (see Lotz et al. 2004). Some predictions of simple dynamical friction calculations do not agree with the observations (Lotz et al. 2001) so additional observations and more sophisticated modeling are needed.

5. Conclusions

This paper has explored the globular cluster luminosity functions and specific frequencies for the full sample of 69 galaxies in the *HST* WFPC2 dE Snapshot Survey. The data has been combined with new complementary surveys of star clusters in a wide range of galaxy types. The main results are:

1. The GCLFs of the dEs in the present sample are well-represented with a t_5 function. The metallicity-corrected peak of the GCLF for Virgo dEs is $M^0_{V,Z}(dE, HST) = -7.3 \pm 0.1$. This is consistent with most other recent measurements of the GCLF peaks in dEs. This result along with recent results from the literature give a fairly clear indication that the GCLF peak in dEs is fainter by ~ 0.3 magnitudes, on average, than the metal-poor peak in spirals and giant ellipticals. This is suggestive that less GC destruction has occurred in dwarfs but more data is needed to confirm this result.

2. The bright-end slope of the luminosity distribution has a power-law form with slope $\alpha = -1.9 \pm 0.1$, consistent with the bright-end slope in most previous studies and with the slope of the mass function of young, luminous clusters in starbursting systems.

3. The trend of increasing $S_{\rm N}$ with decreasing luminosity seen in earlier studies is confirmed. Likewise, we continue to see that dE,N galaxies have a mean value of $S_{\rm N}$ about a factor of two higher than the mean for dE,noN galaxies.

4. In order to compare the metal-poor GCSs of different types of galaxies we compute $T_{\rm MP}$, the number of GCs normalized to galaxy mass. All galaxies with $\log(M/M_\odot) < 10.5$ show a consistent trend of increasing $T_{\rm MP}$ with decreasing galaxy mass. The slope of

the trend in $T_{\rm MP}$ is consistent with the SNe-wind models of Dekel & Silk (1986) and McLaughlin (1999).

5. Assuming a universal GCLF the percentage of stellar mass in GCs is $F_{\rm MP} = 0.0433 T_{\rm MP}$. For galaxies that have formed GCs, $F_{\rm MP}$ ranges from 0.02 for spirals and low-luminosity ellipticals to about 10 for the faintest dwarfs.

Recent large, uniform surveys of star cluster systems in all types of galaxies, dwarf galaxies in particular, are starting to reveal more clearly the complicated interaction between cluster formation, the feedback of that formation on the evolution of galaxies, and the importance of environments. While the cluster mass function appears to be universal within the uncertainties, there is growing evidence that the bend in the GCLF of dwarf galaxies is at a lower luminosity, or mass, than in giant galaxies due to less dynamical evolution. It is still uncertain whether the GCLF of low mass galaxies is a nearly pristine power law. Also, clearly feedback and galaxy mass are fundamental parameters. Theories of supernovae driven winds can explain the tends of $T_{\rm MP}$ with galaxy mass and show that low-mass galaxies will have difficulty retaining the products of star formation. This also explains why higher mass dwarfs have a higher fraction of redder, more metal-rich star clusters (Strader et al. 2006; Peng et al. 2006). However, the differences in $T_{\rm MP}$ and the spatial distributions of dE,N and dE,noN galaxies also indicate the importance of environment (i.e. cluster core, cluster outskirts, or field).

While this work has illuminated some of the fundamental processes of star cluster formation, (i.e. the shape of the cluster mass function and the dependence of $T_{\rm MP}$ and $F_{\rm MP}$ on host galaxy mass), future work is needed to constrain cluster formation histories and their dependence on environment. The ages and metallicities either measured directly or inferred from colors suggest a common period of star cluster formation in all galaxy types and environments very soon after the first stars began to form. However, as explained in general terms by theories and simulations of galaxy and structure formation, a given potential well in a high density environment can collapse earlier and have a higher average star formation rates than the same potential in a low-density environments. This picture predicts that star clusters formed in high-density environments should be slightly older than those formed in low-density environments. This may be seen in globular clusters in the Milky Way that are thought to have been accreted from dwarf galaxies (Mackey & Gilmore 2004). More accurate abundances, [α/Fe] ratios, and ages of a wide sample of star clusters and nuclei are needed to confirm these predictions. Surveying star clusters in dwarf galaxies is a demonstrated fruitful approach to studying the formation and evolution of both star clusters and galaxies.

We would like to thank the referee for useful suggestions and Dean McLaughlin for useful discussions about this work. This research has made use of NASA's Astrophysics Data System Bibliographic Services and the NASA/IPAC Extragalactic Database (NED) which is operated by the Jet Propulsion Laboratory, California Institute of Technology, under contract with the National Aeronautics and Space Administration. B. W. M. is supported by the Gemini Observatory, which is operated by the Association of Universities for Research in Astronomy, Inc., on behalf of the international Gemini partnership of Argentina, Australia, Brazil, Canada, Chile, the United Kingdom, and the United States of America. J. M. L. acknowledges support from the NOAO Leo Goldberg Fellowship.

REFERENCES

Alonso-Herrero, A., Takagi, T., Baker, A. J., Rieke, G. H., Rieke, M. J., Imanishi, M., & Scoville, N. Z. 2004, ApJ, 612, 222

Ashman, K. M., Conti, A., & Zepf, S. E. 1995, AJ, 110, 1164

Baumgardt, H. 1998, A&A, 330, 480

Beasley, M. A., Baugh, C. M., Forbes, D. A., Sharples, R. M., & Frenk, C. S. 2002, MNRAS, 333, 383

Beasley, M. A., Strader, J., Brodie, J. P., Cenarro, A. J., & Geha, M 2006, AJ, 131, 814

Bekki, K., Couch, W. J., & Shioya, Y. 2006, ApJ, 642, L133

Bekki, K., Yahagi, H., & Forbes, D. A. 2006, ApJ, 645, L29

Billett, O. H., Hunter, D. A., & Elmegreen, B. G. 2002, AJ, 123, 1454

Binggeli, B., Sandage, A., & Tammann, G. A. 1985, AJ, 90, 1681

Bruzual, G., & Charlot, S. 2003, MNRAS, 344, 1000

Chandar, R., Whitmore, B., & Lee, M. G. 2004, ApJ, 611, 220

Côté, P., Marzke, R. O., & West, M. J. 1998, 501, 554

Côté, P., et al. 2004, ApJS, 153, 223

Côté, P., et al. 2006, ApJS, 165, 57

Da Costa, G. S., & Mould, J. R. 1988, ApJ, 334, 159

de Grijs, R., Wilkinson, M. I., & Tadhunter, C. N. 2005, MNRAS, 361, 311

Dekel, A., & Birnboim, Y. 2004, AIP Conf. Proc. 743: The New Cosmology: Conference on Strings and Cosmology, 743, 162

Dekel, A., & Silk, J. 1986, ApJ, 303, 39

Di Criscienzo, M., Caputo, F., Marconi, M., & Musella, I. 2006, MNRAS, 365, 1357

Durrell, P. R., Harris, W. E., Geisler, D., & Pudritz, R. E. 1996, AJ, 112, 972

Elmegreen, B. G., & Efremov, Y. N. 1997, ApJ, 480, 235

Faber, S. M., & Gallagher, J. S. 1979, ARA&A, 17, 135

Fall, S. M., & Rees, M. J. 1985, ApJ, 298, 18

Fall, S. M., & Zhang, Q. 2001, ApJ, 561, 751

Ferguson, H. C. 1989, AJ, 98, 367

Ferguson, H. C., & Sandage, A. 1989, ApJ, 346, L53

Ferguson, H. C., & Sandage, A. 1990, AJ, 100, 1

Fleming, D. E. B., Harris, W. E., Pritchet, C. J., & Hanes, D. A. 1995, AJ, 109, 1044

Forbes, D. A. 2005, ApJ, 635, L137

Freedman, W. L., et al. 2001, ApJ, 553, 47

Geha, M., Guhathakurta, P., & van der Marel, R. P. 2002, AJ, 124, 3073

Goudfrooij, P., Strader, J., Brenneman, L., Kissler-Patig, M., Minniti, D., & Edwin Huizinga, J. 2003, MNRAS, 343, 665

Goudfrooij, P., Gilmore, D., Whitmore, B. C., & Schweizer, F. 2004, ApJ, 613, L121

Gnedin, O. Y., & Ostriker, J. P. 1997, ApJ, 474 223

Graham, A. W., & Guzman, R. 2003, AJ, 125, 2936

Harris, W. E. 1991, ARA&A, 29, 543

Harris, W. E., & Pudritz, R. E. 1994, ApJ, 429, 177

Harris, W. E., & van den Bergh, S. 1981, AJ, 86, 1627

Holtzman J. A. et al. 1992, AJ, 103, 691

Hernandez, X., & Gilmore, G. 1998, MNRAS, 297, 517

Jerjen, H., Binggeli, B., & Barazza, F. D. 2004, AJ, 127, 771

Jordán, A., et al. 2005, ApJ, 634, 1002

Jordán, A., et al. 2006, ApJ, 651, L25

Jordán, A., et al. 2007a, ApJS, 169, 213

Jordán, A., et al. 2007b, ApJS, 171, 101

Kissler-Patig, M., Brodie, J. P., Schroder, L. L., Forbes, D. A., Grillmair, C. J., & Huchra, J. P. 1998, AJ, 115, 105

Kundu, A., & Whitmore, B. C. 2001, AJ, 121, 2950

Kravtsov, A. V., & Gnedin, O. Y. 2005, ApJ, 623, 650

Larsen, S. S., Brodie, J. P., Huchra, J. P., Forbes, D. A., & Grillmair, C. J. 2001, AJ, 121, 2974

Lotz, J. M., et al. 2001, ApJ, 552, 572

Lotz, J. M., Miller, B. W., & Ferguson, H. C. 2004, ApJ, 613, 262

Mackey, A. D., & Gilmore, G. F. 2004, MNRAS, 355, 504

Mateo, M. L. 1998, ARA&A, 36, 435

McLaughlin, D. E. 1994, PASP, 106, 47

McLaughlin, D. E. 1999, AJ, 117, 2398

McLaughlin, D. E., & Pudritz, R. E. 1996, ApJ, 457, 578

Miller, B. W., Whitmore, B. C., Schweizer, F., & Fall, S. M. 1997, AJ, 114, 2381

Miller, B. W., Lotz, J. M., Ferguson, H. C., Stiavelli, M., & Whitmore, B. C. 1998, ApJ, 508, L133

Miocchi, P., Capuzzo Dolcetta, R., & Di Matteo, P. 2006, in Globular Clusters, Guide to Galaxies (ESO, Springer-Verlag) (astro-ph/06055008)

Oh, K. S., & Lin, D. N. C. 2000, ApJ, 543, 620

Peng, E. W., et al. 2006, ApJ, 639, 95

Rhode, K. L., Zepf, S. E., & Santos, M. R. 2005, ApJ, 630, L21

Secker, J. 1992, AJ, 104, 1472

Secker, J., & Harris, W. E. 1993, AJ, 105, 1358

Seth, A., Olsen, K., Miller, B., Lotz, J., & Telford, R. 2004, AJ, 127, 798

Schlegel, D. J., Finkbeiner, D. P., & Davis, M. 1998, ApJ, 500, 525

Sharina, M. E., Puzia, T. H., & Makarov, D. I. 2005, A&A, 442, 85

Stiavelli, M., Miller, B. W., Ferguson, H. C., Mack, J., Whitmore, B. C., & Lotz, J. M. 2001, AJ, 121, 1385

Strader, J., Brodie, J. P., Spitler, L., & Beasley, M. A. 2006, AJ, 132, 2333

van den Bergh, S. 2006, AJ, 131, 304

van Zee, L., Barton, E. J., & Skillman, E. D. 2004, AJ, 128, 2797

Vesperini, E. 2000, MNRAS, 318, 841

Vesperini, E. 2001, MNRAS, 322, 247

Vesperini, E., & Zepf, S. E. 2003, ApJ, 587, L97

Whitmore, B. C., Sparks, W. B., Lucas, R. A., Macchetto, F. D., & Biretta, J. A. 1995, ApJ, 454, L73

Whitmore, B. C., Miller, B. W., Schweizer, F., & Fall, S. M. 1997, AJ, 114, 1797

Whitmore, B. C., Zhang, Q., Leitherer, C., Fall, S. M., Schweizer, F., & Miller, B. W. 1999, AJ, 118, 1551

Zepf, S. E., & Ashman, K. M. 1993, MNRAS, 264, 611

Table 1. Basic Properties of Nucleated Galaxies in the *HST* dE Snapshot Survey

Galaxy	Type[a]	RA (J2000)	Dec (J2000)	B[a]	A_B[b]	M_B[c]	N_{GC}[d]
LGC0050	dE,N	10:51:01.60	13:20:01.0	16.7	0.06	−13.36	7.2 ± 3.8
FCC0025	dE0,N	3:23:33.40	-36:59:02.0	17.7	0.00	−13.70	2.5 ± 3.7
FCC0046	dE4	3:26:25.02	-37:07:41.4	15.6	0.00	−15.80	8.0 ± 4.2
FCC0059	dE0,N	3:27:46.60	-33:33:51.0	19.4	0.00	−12.00	0.0 ± 3.2
FCC0136	dE2,N	3:34:29.48	-35:32:47.0	14.8	0.00	−16.60	18.0 ± 5.3
FCC0146	dE4,N	3:35:11.60	-35:19:23.0	19.5	0.00	−11.90	0.5 ± 2.7
FCC0150	dE4,N	3:35:24.09	-36:21:49.6	15.7	0.00	−15.70	8.0 ± 4.2
FCC0174	dE1,N	3:36:45.49	-33:00:50.5	16.7	0.00	−14.70	8.0 ± 3.7
FCC0189	dE4,N	3:37:08.21	-34:43:54.3	18.8	0.00	−12.60	0.5 ± 3.4
FCC0238	dE5,N	3:40:17.19	-36:32:05.5	18.7	0.00	−12.70	2.0 ± 2.0
FCC0242	dE5	3:40:20.54	-37:38:41.0	17.8	0.00	−13.60	0.0 ± 2.7
FCC0246	dE2	3:40:37.70	-36:07:16.0	19.1	0.00	−12.30	0.0 ± 2.7
FCC0254	dE0,N	3:41:00.80	-35:44:33.0	17.6	0.00	−13.80	4.5 ± 4.2
FCC0316	dE3,N	3:47:01.40	-36:26:15.0	16.7	0.00	−14.70	17.0 ± 5.6
FCC0324	dS01(8)	3:47:52.67	-36:28:18.1	15.3	0.00	−16.10	9.0 ± 4.6
VCC0158	dE3,N	12:15:40.07	15:00:20.1	15.8	0.11	−15.21	8.9 ± 4.6
VCC0240	dE2,N	12:17:31.33	14:21:20.4	18.2	0.14	−12.84	7.2 ± 4.1
VCC0452	dE4,N	12:21:04.74	11:45:17.6	15.8	0.01	−15.11	15.5 ± 5.3
VCC0503	dE3,N	12:21:50.24	8:32:27.8	16.8	0.01	−14.11	2.5 ± 3.7
VCC0529	dE4,N	12:22:08.59	9:53:39.9	18.2	0.00	−12.70	3.5 ± 3.5
VCC0646	dE3	12:23:31.80	17:47:40.5	18.8	0.03	−12.13	4.5 ± 3.9
VCC0747	dE0,N	12:24:47.77	8:59:29.2	16.2	0.00	−14.70	14.0 ± 4.9
VCC0871	dE4,N	12:26:05.63	12:33:33.7	15.4	0.09	−15.59	15.6 ± 4.9
VCC0896	dE3,N	12:26:22.48	12:46:59.9	17.8	0.10	−13.20	4.5 ± 3.9
VCC0940	dE1,N	12:26:47.05	12:27:14.6	14.8	0.09	−16.19	52.4 ± 8.1
VCC0949	dE4,N	12:26:54.55	10:39:57.1	15.1	0.00	−15.80	19.7 ± 5.8
VCC0965	dE7,N	12:27:03.30	12:33:37.8	15.4	0.10	−15.60	13.2 ± 4.6
VCC0992	dE0,N	12:27:18.63	8:12:45.5	15.8	0.00	−15.10	3.0 ± 4.1
VCC1073	dE3,N	12:28:08.60	12:05:35.7	14.2	0.07	−16.77	16.7 ± 5.8
VCC1077	dE0,N	12:28:10.36	12:48:24.7	19.2	0.08	−11.78	1.5 ± 4.5

Table 1—Continued

Galaxy	Type[a]	RA (J2000)	Dec (J2000)	B[a]	A_B[b]	M_B[c]	N_{GC}[d]
VCC1105	dE0,N	12:28:27.24	14:09:20.9	16.2	0.08	−14.78	4.1 ± 3.4
VCC1107	dE4,N	12:28:30.55	7:19:29.7	15.1	0.01	−15.81	21.6 ± 5.5
VCC1252	dE0,N	12:30:01.74	9:28:25.7	18.8	0.00	−12.10	6.5 ± 4.2
VCC1254	dE0,N	12:30:05.09	8:04:23.6	15.0	0.00	−15.90	20.5 ± 8.0
VCC1272	dE1,N	12:30:15.54	13:18:25.9	18.5	0.06	−12.46	2.5 ± 3.4
VCC1308	dE6,N	12:30:45.95	11:20:35.5	15.1	0.02	−15.82	7.0 ± 4.3
VCC1311	dE1,N	12:30:47.32	7:36:19.1	15.6	0.00	−15.30	15.7 ± 4.7
VCC1363	dE3,N	12:31:27.84	10:55:50.5	19.0	0.00	−11.90	0.0 ± 2.5
VCC1386	dE3,N	12:31:51.40	12:39:26.0	14.4	0.07	−16.57	22.7 ± 6.1
VCC1497	dE4,N	12:33:18.53	17:27:32.7	15.7	0.04	−15.24	5.0 ± 4.6
VCC1514	dE7,N	12:33:37.72	7:52:16.5	15.1	0.00	−15.80	1.8 ± 2.5
VCC1530	dE2,N	12:33:55.69	5:43:07.6	18.3	0.00	−12.60	6.5 ± 4.2
VCC1577	dE4	12:34:38.37	15:36:09.7	15.8	0.02	−15.12	12.5 ± 5.0
VCC1714	dE4,N	12:37:25.65	14:18:48.3	18.5	0.03	−12.43	0.0 ± 3.8
VCC1876	dE5,N	12:41:20.42	14:42:01.9	14.9	0.03	−16.03	22.1 ± 6.3

[a]Morphological types and apparent B magnitudes taken from the following catalogs: FCC = Fornax Cluster Catalog (Ferguson 1989); VCC = Virgo Cluster Catalog (Binggeli et al. 1985); LGC = Leo Group Catalog (Ferguson & Sandage 1990).

[b]Foreground extinction from Schlegel et al. (1998) as reported in the NASA Extragalactic Database (NED).

[c]Absolute B magnitudes, corrected for foreground extinction, calculated assuming $(m - M)_0 = 30.0$ for the Leo Group, 30.92 for the Virgo Cluster, and 31.39 for the Fornax Cluster (Freedman et al. 2001).

[d]Corrected for background contamination. From Lotz et al. (2004) with galaxy association corrected.

Table 2. Basic Properties of Non-nucleated Galaxies in the *HST* dE Snapshot Survey

Galaxy	Type[a]	RA (J2000)	Dec (J2000)	B[a]	A_B[b]	M_B[c]	N_{GC}[d]
LGC0047	dE	10:50:18.97	13:16:21.1	14.9	0.06	−15.16	2.9 ± 4.4
FCC0027	dE2	3:23:55.76	-34:48:26.5	19.3	0.00	−12.10	0.5 ± 3.1
FCC0048	dE3	3:26:42.55	-34:32:49.9	17.1	0.00	−14.30	7.0 ± 4.4
FCC0064	dE5	3:28:00.49	-38:32:15.1	17.5	0.00	−13.90	0.0 ± 2.9
FCC0110	dE4	3:32:57.37	-35:44:15.5	16.8	0.00	−14.60	0.0 ± 4.2
FCC0144	dE0	3:35:00.30	-35:19:20.0	19.2	0.00	−12.20	0.5 ± 3.4
FCC0212	dE1?	3:38:20.90	-36:24:42.0	17.6	0.00	−13.80	5.5 ± 5.3
FCC0218	dE4	3:38:45.40	-35:15:59.0	18.5	0.00	−12.90	0.0 ± 2.7
FCC0304	dE1	3:45:30.90	-34:30:18.0	18.8	0.00	−12.60	0.0 ± 3.1
VCC0009	dE1,N	12:09:22.34	13:59:33.1	13.9	0.02	−17.02	23.9 ± 6.9
VCC0118	dE3	12:14:36.85	9:41:21.8	15.6	0.00	−15.30	3.0 ± 3.6
VCC0128	dE0	12:14:59.51	9:33:55.0	15.6	0.00	−15.30	11.1 ± 4.3
VCC0543	dE5	12:22:19.53	14:45:38.3	14.8	0.08	−16.18	12.9 ± 4.4
VCC0546	dE6	12:22:21.59	10:36:07.1	15.7	0.03	−15.23	4.8 ± 3.3
VCC0917	dE6	12:26:32.37	13:34:43.5	14.9	0.11	−16.11	6.0 ± 5.1
VCC0996	dE5	12:27:21.17	13:06:36.3	18.4	0.09	−12.59	0.0 ± 3.7
VCC1651	dE5	12:36:07.46	6:03:17.4	17.0	0.00	−13.90	4.2 ± 5.3
VCC1729	dE5?	12:37:46.06	10:59:07.1	17.8	0.00	−13.10	1.0 ± 3.0
VCC1762	dE6	12:38:32.18	10:22:35.6	16.2	0.00	−14.70	4.0 ± 3.5
VCC1781	dE4	12:39:11.77	8:04:25.5	18.7	0.00	−12.20	2.5 ± 3.4
VCC1877	dE2	12:41:24.22	8:21:57.1	18.6	0.00	−12.30	3.0 ± 3.3
VCC1948	dE3	12:42:58.02	10:40:54.5	15.1	0.00	−15.80	6.5 ± 3.7
VCC2008	dE5	12:44:47.48	12:03:51.5	15.1	0.01	−15.81	7.5 ± 5.1
VCC2029	dE3	12:45:40.60	9:24:18.6	18.2	0.02	−12.72	1.0 ± 3.6

[a]Morphological types and apparent B magnitudes taken from the following catalogs: FCC = Fornax Cluster Catalog (Ferguson 1989); VCC = Virgo Cluster Catalog (Binggeli et al. 1985); LGC = Leo Group Catalog (Ferguson & Sandage 1990).

[b]Foreground extinction from Schlegel et al. (1998) as reported in the NASA Extragalactic Database (NED).

[c]Absolute B magnitudes, corrected for foreground extinction, calculated assuming $(m - M)_0 = 30.0$ for the Leo Group, 30.92 for the Virgo Cluster, and 31.39 for the Fornax Cluster (Freedman et al. 2001).

[d]Corrected for background contamination. From Lotz et al. (2004) with galaxy association corrected.

Table 3. V-band GCLF for all Virgo galaxies

V (1)	N_{GC+nuc} (2)	$f_{bkg,GC+nuc}$ (3)	N_{GC} (4)	$f_{bkg,GC}$ (5)
17.666	2.1 ± 1.4	0.90	2.0 ± 1.4	1.00
17.998	3.0 ± 1.7	0.89	2.9 ± 1.7	0.89
18.330	2.1 ± 1.4	0.78	2.0 ± 1.4	0.89
18.662	2.1 ± 1.4	0.71	0.9 ± 0.9	0.83
18.994	4.0 ± 2.0	0.40	4.0 ± 2.0	0.50
19.326	3.0 ± 1.7	0.50	2.9 ± 1.7	0.50
19.658	7.0 ± 2.6	0.74	6.0 ± 2.5	0.79
19.990	4.9 ± 2.2	0.50	4.9 ± 2.2	0.54
20.322	10.0 ± 3.2	0.48	10.1 ± 3.2	0.57
20.654	7.0 ± 2.6	0.42	6.0 ± 2.5	0.50
20.986	7.9 ± 2.8	0.43	6.9 ± 2.6	0.50
21.318	9.1 ± 3.0	0.21	6.0 ± 2.5	0.26
21.650	13.0 ± 3.6	0.36	12.1 ± 3.5	0.40
21.982	22.1 ± 4.7	0.22	18.1 ± 4.3	0.26
22.314	36.1 ± 6.0	0.20	33.1 ± 5.8	0.22
22.646	44.9 ± 6.7	0.21	42.9 ± 6.5	0.23
22.978	68.0 ± 8.2	0.19	63.9 ± 8.0	0.20
23.310	74.0 ± 8.6	0.23	71.1 ± 8.4	0.23
23.642	81.9 ± 9.1	0.27	81.1 ± 9.0	0.27
23.974	81.9 ± 9.1	0.30	80.0 ± 8.9	0.31
24.306	91.9 ± 9.6	0.48	90.9 ± 9.5	0.49
24.638	74.9 ± 8.7	0.64	75.1 ± 8.7	0.65
24.970	46.1 ± 6.8	0.73	46.0 ± 6.8	0.75
25.302	4.0 ± 2.0	0.73	4.0 ± 2.0	0.77

Note. — (1) V magnitude of bin center; (2) Total GC+nuclei in bin (histogram in Figure 2a), $\phi(V) \times 701 \times 0.332$ with Poisson errors; (3) Background fraction of objects in (2); (4) Like (2) but GC candidates only,

$\phi(V) \times 673 \times 0.332$; (5) Background fraction of objects in (4).

Table 4. V-band GCLF for all Fornax galaxies

V (1)	N_{GC+nuc} (2)	$f_{bkg,GC+nuc}$ (3)	N_{GC} (4)	$f_{bkg,GC}$ (5)
17.666	0.0 ± 0.0	1.00	0.0 ± 0.0	1.00
17.998	2.0 ± 1.4	0.94	2.0 ± 1.4	1.00
18.330	0.0 ± 0.0	0.92	0.0 ± 0.0	1.00
18.662	0.0 ± 0.0	0.89	0.0 ± 0.0	1.00
18.994	0.0 ± 0.0	0.80	0.0 ± 0.0	1.00
19.326	2.0 ± 1.4	0.83	1.0 ± 1.0	1.00
19.658	1.0 ± 1.0	0.95	1.0 ± 1.0	0.97
19.990	2.0 ± 1.4	0.85	1.0 ± 1.0	1.00
20.322	2.0 ± 1.4	0.85	1.0 ± 1.0	0.99
20.654	1.0 ± 1.0	0.84	0.0 ± 0.0	0.96
20.986	1.0 ± 1.0	0.83	1.0 ± 1.0	0.94
21.318	2.0 ± 1.4	0.64	2.0 ± 1.4	0.90
21.650	4.0 ± 2.0	0.78	2.0 ± 1.4	0.93
21.982	4.0 ± 2.0	0.62	2.0 ± 1.4	0.84
22.314	4.0 ± 2.0	0.57	3.0 ± 1.7	0.76
22.646	9.0 ± 3.0	0.56	7.0 ± 2.7	0.71
22.978	9.0 ± 3.0	0.50	9.0 ± 3.0	0.59
23.310	16.0 ± 4.0	0.51	15.0 ± 3.9	0.54
23.642	21.0 ± 4.6	0.52	21.0 ± 4.6	0.51
23.974	29.0 ± 5.4	0.51	27.0 ± 5.2	0.49
24.306	24.0 ± 4.9	0.65	24.0 ± 4.9	0.66
24.638	31.0 ± 5.6	0.74	31.0 ± 5.6	0.80
24.970	25.0 ± 5.0	0.75	25.0 ± 5.0	0.85
25.302	9.0 ± 3.0	0.68	9.0 ± 3.0	0.84

Note. — (1) V magnitude of bin center; (2) Total GC+nuclei in bin (histogram in Figure 2b), $\phi(V) \times 198 \times 0.332$; (3) Background fraction of objects in (2); (4) Like (2) but GC candidates only, $\phi(V) \times 184 \times 0.332$; (5) Back-

ground fraction of objects in (4).

Table 5. I-band GCLF (GC + nuclei) for Virgo and Fornax galaxies

I (1)	N_{Virgo} (2)	$f_{bkg,Virgo}$ (3)	N_{Fornax} (4)	$f_{bkg,Fornax}$ (5)
16.686	3.1 ± 1.8	1.00	1.0 ± 1.0	0.96
17.058	2.1 ± 1.4	1.00	1.0 ± 1.0	1.00
17.430	1.0 ± 1.0	0.90	0.0 ± 0.0	0.94
17.802	3.1 ± 1.8	0.95	0.0 ± 0.0	0.89
18.174	2.1 ± 1.4	0.73	0.0 ± 0.0	1.00
18.546	8.1 ± 2.8	0.81	2.0 ± 1.4	0.96
18.918	6.0 ± 2.4	0.70	2.0 ± 1.4	0.86
19.290	7.0 ± 2.7	0.72	2.0 ± 1.4	0.92
19.662	12.0 ± 3.5	0.50	1.0 ± 1.0	0.84
20.034	8.1 ± 2.8	0.56	3.0 ± 1.7	0.86
20.406	14.1 ± 3.8	0.40	1.0 ± 1.0	0.81
20.778	15.1 ± 3.9	0.29	8.0 ± 2.8	0.72
21.150	27.9 ± 5.3	0.26	3.0 ± 1.7	0.69
21.522	42.0 ± 6.5	0.15	5.0 ± 2.2	0.53
21.894	63.1 ± 7.9	0.20	11.0 ± 3.3	0.60
22.266	74.1 ± 8.6	0.23	13.0 ± 3.6	0.59
22.638	98.1 ± 9.9	0.27	21.0 ± 4.6	0.56
23.010	99.9 ± 0.0	0.33	32.0 ± 5.7	0.52
23.382	93.1 ± 9.6	0.53	33.0 ± 5.7	0.62
23.754	92.1 ± 9.6	0.68	31.0 ± 5.6	0.69
24.126	30.0 ± 5.5	0.73	24.0 ± 4.9	0.79
24.498	0.0 ± 0.0	0.19	4.0 ± 2.0	0.46

Note. — (1) I magnitude of bin center; (2) Total Virgo GC+nuclei in bin, $\phi(I) \times 701 \times 0.372$ (histogram in Figure 3a); (3) Background fraction of objects in (2); (4) Like (2) but for Fornax galaxies, $\phi(V) \times 198 \times 0.372$ (histogram

in Figure 3b); (5) Background fraction of objects in (4).

Table 6. Best-fitting Parameters of dE GCLFs

Sample	m^0	σ_t[a]	M^{0}[b]
V-band			
Virgo (GC+nuclei)	23.61 ± 0.11	1.08 ± 0.09	-7.31 ± 0.11
Virgo (GC only)	23.63 ± 0.09	1.02 ± 0.09	-7.29 ± 0.10
Virgo (dE,N, GC only)	23.69 ± 0.11	1.06 ± 0.10	-7.23 ± 0.11
Virgo (dE,noN, GC only)	23.42 ± 0.17	0.77 ± 0.18	-7.50 ± 0.17
Virgo bright (GC+nuc)	23.64 ± 0.09	0.97 ± 0.08	-7.28 ± 0.09
Virgo faint (GC+nuc)	23.18 ± 0.43	1.63 ± 0.30	-7.74 ± 0.43
Fornax (GC+nuclei)	24.15 ± 0.40	1.03 ± 0.30	-7.24 ± 0.40
Fornax (GC only)	24.00 ± 0.28	0.67 ± 0.23	-7.39 ± 0.30
Nuclei	21.26 ± 0.21	1.11 ± 0.18	-9.7 ± 0.2
I-band			
Virgo (GC+nuclei)	22.80 ± 0.11	1.1 ± 0.1	-8.12 ± 0.11
Fornax (GC+nuclei)	23.40 ± 0.40	1.0 ± 0.3	-8.00 ± 0.40

[a]Equivalent Gaussian sigma: $\sigma_G \approx 1.29\sigma_t$.

[b]Assuming $(m-M)_0^{Virgo} = 30.92$, $(m-M)_0^{Fornax} = 31.39$

Table 7. GCLF Parameter Simulations

Galaxy σ_D	V^{0}[a]	σ_t[b]
1.0 Mpc	23.59 ± 0.09	1.11 ± 0.05
2.0 Mpc	23.59 ± 0.08	1.13 ± 0.04
3.0 Mpc	23.56 ± 0.08	1.18 ± 0.03
4.0 Mpc	23.52 ± 0.12	1.23 ± 0.06

[a]Input value is 23.62

[b]Input value is 1.1

Table 8. V-band GCLF for Virgo galaxies with $M_V > -15.75$

V (1)	N_{GC+nuc} (2)	$f_{bkg,GC+nuc}$ (3)	N_{GC} (4)	$f_{bkg,GC}$ (5)
17.666	0.0 ± 0.0	0.83	0.0 ± 0.0	0.80
17.998	0.0 ± 0.0	0.76	0.0 ± 0.0	0.77
18.330	0.0 ± 0.0	0.71	0.0 ± 0.0	0.68
18.662	0.0 ± 0.0	0.54	0.0 ± 0.0	0.55
18.994	4.0 ± 2.0	0.32	4.0 ± 2.0	0.31
19.326	0.0 ± 0.0	0.29	0.0 ± 0.0	0.30
19.658	2.0 ± 1.4	0.63	2.0 ± 1.4	0.62
19.990	2.0 ± 1.4	0.37	2.0 ± 1.4	0.37
20.322	3.0 ± 1.7	0.40	3.0 ± 1.7	0.44
20.654	2.0 ± 1.4	0.38	2.0 ± 1.4	0.42
20.986	4.0 ± 2.0	0.42	4.0 ± 2.0	0.47
21.318	7.0 ± 2.6	0.24	4.0 ± 2.0	0.29
21.650	6.0 ± 2.5	0.43	5.0 ± 2.2	0.51
21.982	9.0 ± 3.0	0.32	6.0 ± 2.4	0.39
22.314	4.0 ± 2.0	0.34	3.0 ± 1.7	0.42
22.646	8.0 ± 2.8	0.41	7.0 ± 2.6	0.49
22.978	16.0 ± 4.0	0.43	14.0 ± 3.7	0.50
23.310	14.0 ± 3.7	0.52	12.0 ± 3.5	0.58
23.642	21.0 ± 4.6	0.60	21.0 ± 4.6	0.65
23.974	18.0 ± 4.2	0.64	18.0 ± 4.2	0.68
24.306	24.0 ± 4.9	0.78	24.0 ± 4.9	0.80
24.638	19.0 ± 4.4	0.86	19.0 ± 4.4	0.86
24.970	17.0 ± 4.1	0.90	17.0 ± 4.1	0.89
25.302	3.0 ± 1.7	0.89	3.0 ± 1.7	0.88

Note. — (1) V magnitude of bin center; (2) Total GC+nuclei in bin, $\phi(V) \times 183 \times 0.332$ (histogram in Figure 5b); (3) Background fraction of objects in (2); (4) Like (2) but GC candidates only, $\phi(V) \times 170 \times 0.332$; (5)

Background fraction of objects in (4).

Table 9. Derived GCS Properties for dE,N in the *HST* dE Snapshot Survey

Galaxy	M_V	$N_{\rm GC}$(tot)	$S_{\rm N}$	$T_{\rm MP}$	$F_{\rm MP}$
LGC0050	-14.13	7.5 ± 4.0	16.6 ± 8.9	39.2 ± 21.0	1.1 ± 0.9
FCC0025	-14.47	3.1 ± 4.5	5.0 ± 7.4	11.9 ± 17.5	0.7 ± 0.2
FCC0046	-16.57	9.9 ± 5.3	2.3 ± 1.2	5.5 ± 2.9	0.2 ± 0.1
FCC0059	-12.77	0.0 ± 4.0	$0. \pm 31.2$	0.0 ± 73.7	0.0 ± 1.7
FCC0136	-17.37	22.3 ± 6.6	2.5 ± 0.7	5.9 ± 1.7	0.2 ± 0.1
FCC0146	-12.67	0.6 ± 3.4	5.3 ± 29.0	12.5 ± 68.5	0.5 ± 0.0
FCC0150	-16.47	9.9 ± 5.3	2.6 ± 1.4	6.0 ± 3.2	0.3 ± 0.0
FCC0174	-15.47	9.9 ± 4.6	6.4 ± 3.0	15.2 ± 7.1	0.4 ± 0.4
FCC0189	-13.37	0.6 ± 4.2	2.8 ± 18.9	6.6 ± 44.5	0.8 ± 0.8
FCC0238	-13.47	2.5 ± 2.5	10.1 ± 10.1	23.9 ± 23.9	0.9 ± 0.1
FCC0242	-14.37	0.0 ± 3.3	0.0 ± 5.9	0.0 ± 13.9	0.0 ± 0.2
FCC0246	-13.07	0.0 ± 3.4	0.0 ± 20.1	0.0 ± 47.4	0.0 ± 0.8
FCC0254	-14.57	5.6 ± 5.2	8.3 ± 7.7	19.5 ± 18.2	0.6 ± 0.3
FCC0316	-15.47	21.1 ± 6.9	13.7 ± 4.5	32.3 ± 10.5	0.9 ± 0.7
FCC0324	-16.87	11.2 ± 5.7	2.0 ± 1.0	4.7 ± 2.4	0.1 ± 0.1
VCC0158	-15.98	10.4 ± 5.4	4.2 ± 2.2	10.0 ± 5.1	0.4 ± 0.1
VCC0240	-13.61	8.5 ± 4.8	30.4 ± 17.2	71.8 ± 40.7	2.8 ± 0.4
VCC0452	-15.88	18.1 ± 6.2	8.1 ± 2.8	19.1 ± 6.6	0.6 ± 0.4
VCC0503	-14.88	2.9 ± 4.3	3.3 ± 4.8	7.7 ± 11.3	0.5 ± 0.2
VCC0529	-13.47	4.1 ± 4.1	16.8 ± 16.9	39.6 ± 39.9	2.9 ± 1.7
VCC0646	-12.9	5.3 ± 4.6	36.5 ± 31.9	86.1 ± 75.3	4.8 ± 1.6
VCC0747	-15.47	16.4 ± 5.7	10.6 ± 3.7	25.1 ± 8.8	0.8 ± 0.4
VCC0871	-16.36	18.2 ± 5.8	5.2 ± 1.7	12.3 ± 3.9	0.4 ± 0.2
VCC0896	-13.97	5.3 ± 4.6	13.6 ± 11.9	32.1 ± 28.1	1.8 ± 0.5
VCC0940	-16.96	61.4 ± 9.5	10.1 ± 1.6	23.8 ± 3.7	0.8 ± 0.3
VCC0949	-16.57	23.1 ± 6.9	5.4 ± 1.6	12.8 ± 3.8	0.4 ± 0.2
VCC0965	-16.37	15.4 ± 5.3	4.4 ± 1.5	10.3 ± 3.6	0.6 ± 0.2
VCC0992	-15.87	3.5 ± 4.8	1.6 ± 2.2	3.7 ± 5.1	0.3 ± 0.2
VCC1073	-17.54	19.6 ± 6.8	1.9 ± 0.7	4.4 ± 1.5	0.2 ± 0.0
VCC1077	-12.55	1.8 ± 5.3	16.8 ± 50.7	39.6 ± 119.6	2.6 ± 1.3

Table 9—Continued

Galaxy	M_V	$N_{\rm GC}$(tot)	$S_{\rm N}$	$T_{\rm MP}$	$F_{\rm MP}$
VCC1105	-15.55	4.8 ± 4.0	2.9 ± 2.4	6.9 ± 5.7	0.6 ± 0.4
VCC1107	-16.58	25.3 ± 6.5	5.9 ± 1.5	13.9 ± 3.6	0.5 ± 0.2
VCC1252	-12.87	7.6 ± 4.9	54.1 ± 34.8	127.8 ± 82.2	5.0 ± 0.8
VCC1254	-16.67	24.0 ± 9.3	5.2 ± 2.0	12.2 ± 4.7	0.7 ± 0.2
VCC1272	-13.23	2.9 ± 4.0	14.9 ± 20.3	35.3 ± 47.8	1.6 ± 0.1
VCC1308	-16.59	8.2 ± 5.1	1.9 ± 1.2	4.5 ± 2.8	0.3 ± 0.2
VCC1311	-16.07	18.4 ± 5.5	6.9 ± 2.1	16.2 ± 4.9	0.7 ± 0.0
VCC1363	-12.67	0.0 ± 3.0	0.0 ± 25.5	0.0 ± 60.3	0.0 ± 0.4
VCC1386	-17.34	26.6 ± 7.2	3.1 ± 0.8	7.3 ± 2.0	0.3 ± 0.0
VCC1497	-16.01	5.8 ± 5.4	2.3 ± 2.1	5.4 ± 5.0	0.2 ± 0.1
VCC1514	-16.57	2.1 ± 2.9	0.5 ± 0.7	1.2 ± 1.6	0.1 ± 0.0
VCC1530	-13.37	7.6 ± 4.9	34.2 ± 22.0	80.6 ± 51.8	3.1 ± 0.5
VCC1577	-15.89	14.6 ± 5.9	6.4 ± 2.6	15.2 ± 6.1	0.6 ± 0.2
VCC1714	-13.2	0.0 ± 4.5	0.0 ± 23.5	0.0 ± 55.6	0.0 ± 0.3
VCC1876	-16.8	25.9 ± 7.4	4.9 ± 1.4	11.7 ± 3.3	0.4 ± 0.2

Table 10. Derived GCS Properties for dE,noN in the *HST* dE Snapshot Survey

Galaxy	M_V	$N_{\rm GC}$(tot)	$S_{\rm N}$	$T_{\rm MP}$	$F_{\rm MP}$
LGC0047	-15.93	3.0 ± 4.5	1.3 ± 1.9	3.0 ± 4.5	0.1 ± 0.0
FCC0027	-12.87	0.6 ± 3.8	4.4 ± 27.1	10.4 ± 64.1	1.5 ± 1.5
FCC0048	-15.07	8.7 ± 5.4	8.1 ± 5.1	19.2 ± 12.0	0.5 ± 0.5
FCC0064	-14.67	0.0 ± 3.6	0.0 ± 4.9	0.0 ± 11.6	0.0 ± 0.3
FCC0110	-15.37	0.0 ± 5.2	0.0 ± 3.7	0.0 ± 8.7	0.0 ± 0.4
FCC0144	-12.97	0.6 ± 4.2	4.0 ± 27.2	9.5 ± 64.3	0.7 ± 0.4
FCC0212	-14.57	6.9 ± 6.6	10.2 ± 9.8	24.0 ± 23.2	1.2 ± 0.2
FCC0218	-13.67	0.0 ± 3.4	0.0 ± 11.6	0.0 ± 27.3	0.0 ± 0.5
FCC0304	-13.37	0.0 ± 3.8	0.0 ± 17.1	0.0 ± 40.4	0.0 ± 0.6
VCC0009	-17.79	28.0 ± 8.1	2.1 ± 0.6	5.1 ± 1.5	0.2 ± 0.0
VCC0118	-16.07	3.5 ± 4.2	1.3 ± 1.6	3.1 ± 3.7	0.1 ± 0.0
VCC0128	-16.07	13.0 ± 5.1	4.9 ± 1.9	11.5 ± 4.5	0.8 ± 0.5
VCC0543	-16.95	15.2 ± 5.1	2.5 ± 0.8	5.9 ± 2.0	0.2 ± 0.0
VCC0546	-16.	5.6 ± 3.9	2.2 ± 1.6	5.3 ± 3.7	0.2 ± 0.1
VCC0917	-16.88	7.0 ± 6.0	1.2 ± 1.1	2.9 ± 2.5	0.2 ± 0.1
VCC0996	-13.36	0.0 ± 4.4	0.0 ± 20.0	0.0 ± 40.0	0.0 ± 0.6
VCC1651	-14.67	4.9 ± 6.2	6.6 ± 8.4	15.7 ± 19.7	0.5 ± 0.2
VCC1729	-13.87	1.2 ± 3.5	3.3 ± 9.9	7.8 ± 23.5	0.6 ± 0.3
VCC1762	-15.47	4.7 ± 4.1	3.0 ± 2.6	7.2 ± 6.2	0.2 ± 0.1
VCC1781	-12.97	2.9 ± 4.0	19.1 ± 25.7	45.0 ± 60.8	7.5 ± 7.8
VCC1877	-13.07	3.5 ± 3.9	20.8 ± 23.0	49.1 ± 54.3	1.8 ± 0.4
VCC1948	-16.57	7.6 ± 4.3	1.8 ± 1.0	4.2 ± 2.4	0.2 ± 0.0
VCC2008	-16.58	8.8 ± 6.0	2.1 ± 1.4	4.9 ± 3.3	0.2 ± 0.0
VCC2029	-13.49	1.2 ± 4.2	4.7 ± 17.0	11.1 ± 40.1	0.4 ± 0.1

Table 11. Mean GCS Properties for Different Galaxy Types

Sample	$S_{\rm N}$	$T_{\rm MP}$	$F_{\rm MP}$	$\langle\log(M_{gal,*})\rangle$
dE,N WFPC2	8.7	20.4	0.9	8.66
dE,noN WFPC2	4.3	10.2	0.7	8.60
dE WFPC2	7.2	16.9	0.8	8.64
dE literature	8.6	21.0	0.9	8.65
dE all	7.6	17.9	0.8	8.64
dE cluster	3.7	16.3	0.7	9.22
dE group	11.3	26.8	1.2	8.14
dI literature	2.6	15.0	0.7	8.23
dI cluster	3.7	21.2	0.9	8.48
dI group	2.0	12.0	0.5	8.12
E/S0	2-10	1.7	0.08	11.41
Spirals	< 2	1.2	0.05	11.17

Table 12. K-S Test Probabilities for $T_{\rm MP}$ in different ranges in log(M)

Sample	P(7.5-8.5)	P(8.5-9.8)	P(7.5-9.8)
dE(N) vs dE(noN)	0.26	0.03	0.03
dE(HST) vs dE(lit)	0.47	0.96	0.71
dE(C) vs dI(Lit)	0.34	0.16	0.03
dE(G) vs dI(Lit)	0.04	0.91	0.27
dE(C) vs dE(G)	0.47	0.07	0.15
dE(C) vs dI(C)	0.93	0.19	0.27
dI(C) vs dI(G)	0.35	0.05	0.03
dE(noN) vs dI(C)	0.93	0.03	0.09
dE(noN) vs dI(G)	0.92	0.07	0.11
dE(noN) vs dI(Lit)	0.93	0.42	0.30
dE(N) vs dI(G)	0.25	0.01	< 0.01
dE(N) vs dI(C)	0.54	0.29	0.64
dE(N) vs dI(Lit)	0.09	0.17	0.05

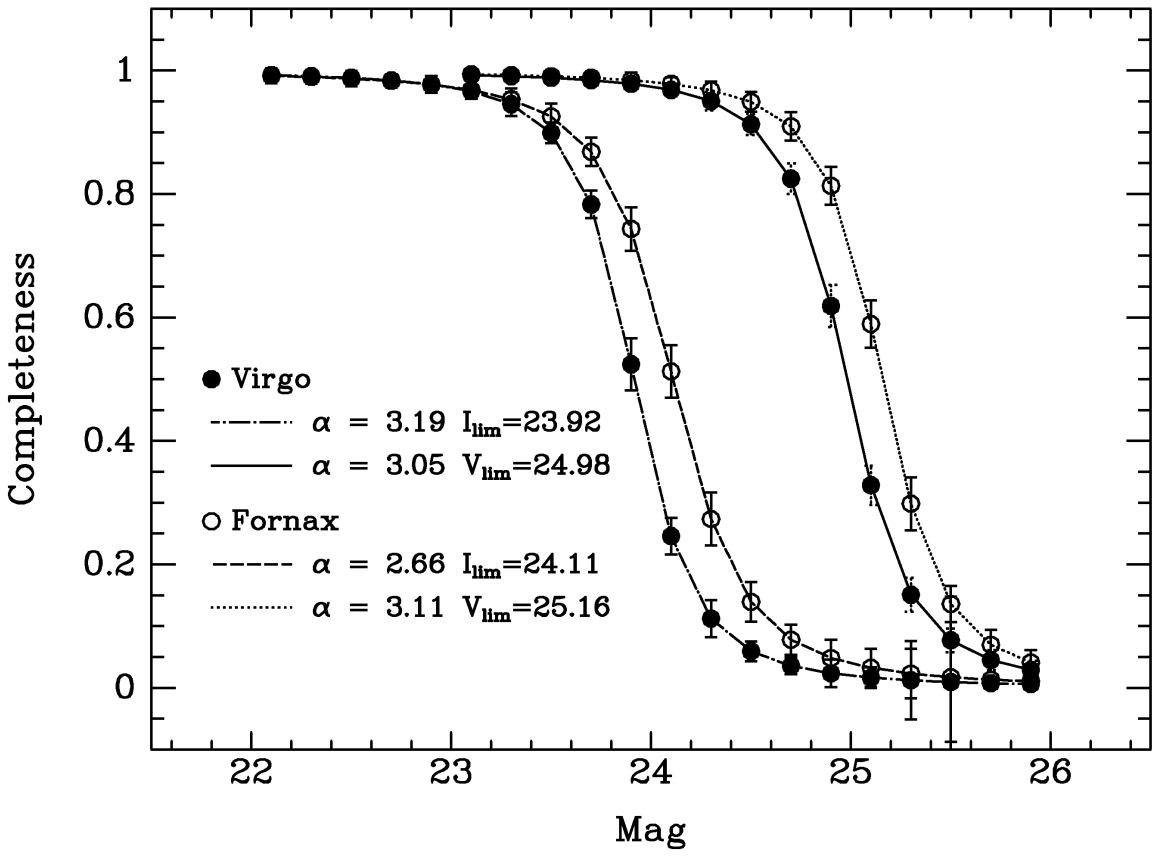

Fig. 1.— The completeness functions of WFPC2 images in the *HST* dE Snapshot Survey. The limiting magnitudes, V_{lim} and I_{lim}, where the completeness fraction drops to 0.5, differs slightly been the Virgo and Fornax Cluster samples. The parameter α from Pritchet's interpolation function (Fleming et al. 1995) is a measure of the sharpness of the drop in the completeness function.

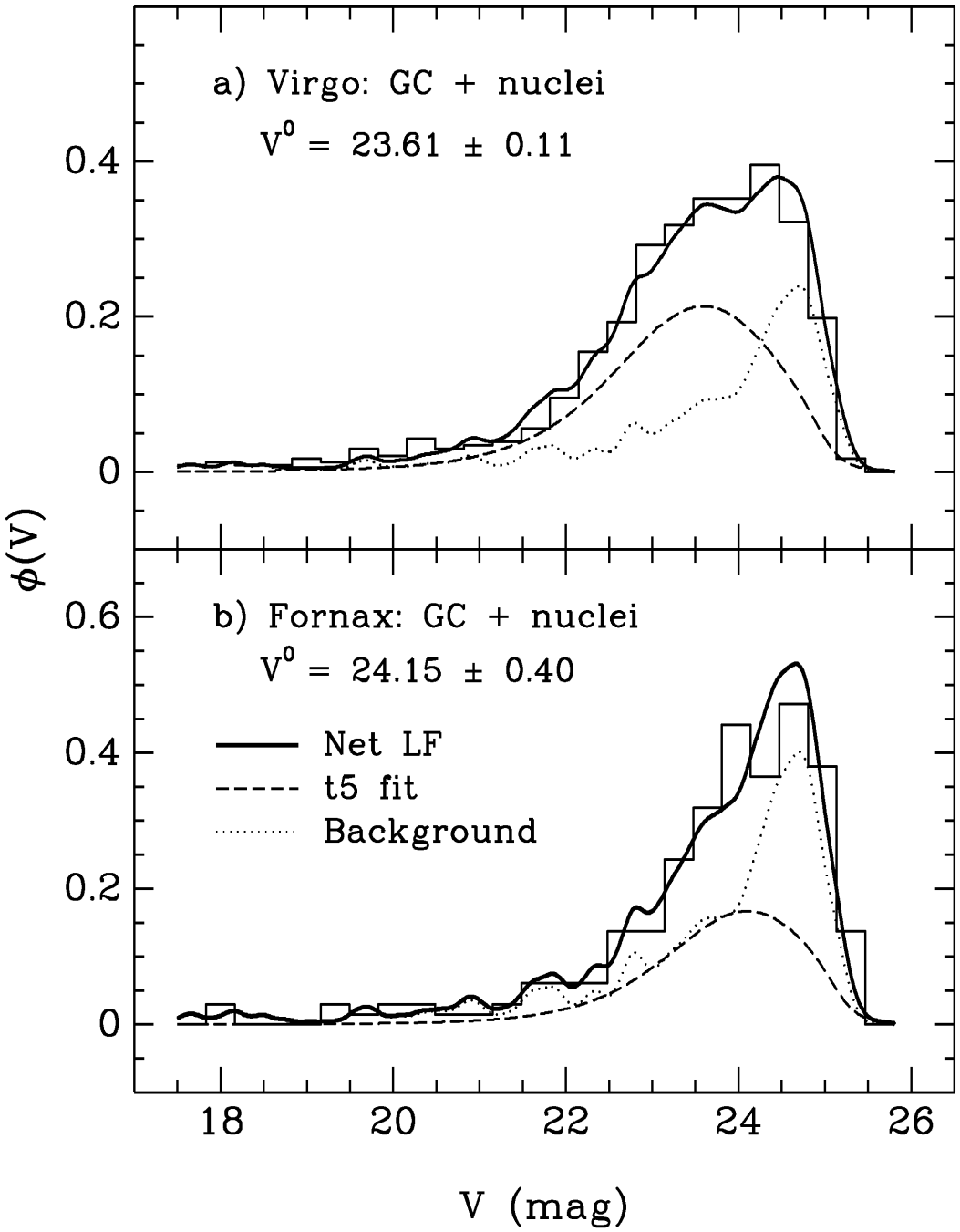

Fig. 2.— V-band GC luminosity functions for the Virgo (a) and Fornax (b) complete samples (GC plus nuclei). The histograms are the LFs for all GC candidates. The dotted curve is the scaled LF of background objects. These values are given in Tables 3 and 4. The dashed curve is the best-fitting t_5 distribution using the method of Secker & Harris (1993) and the dark solid curve is the total fit. All the smooth curves have been convolved with the completeness functions in Figure 1.

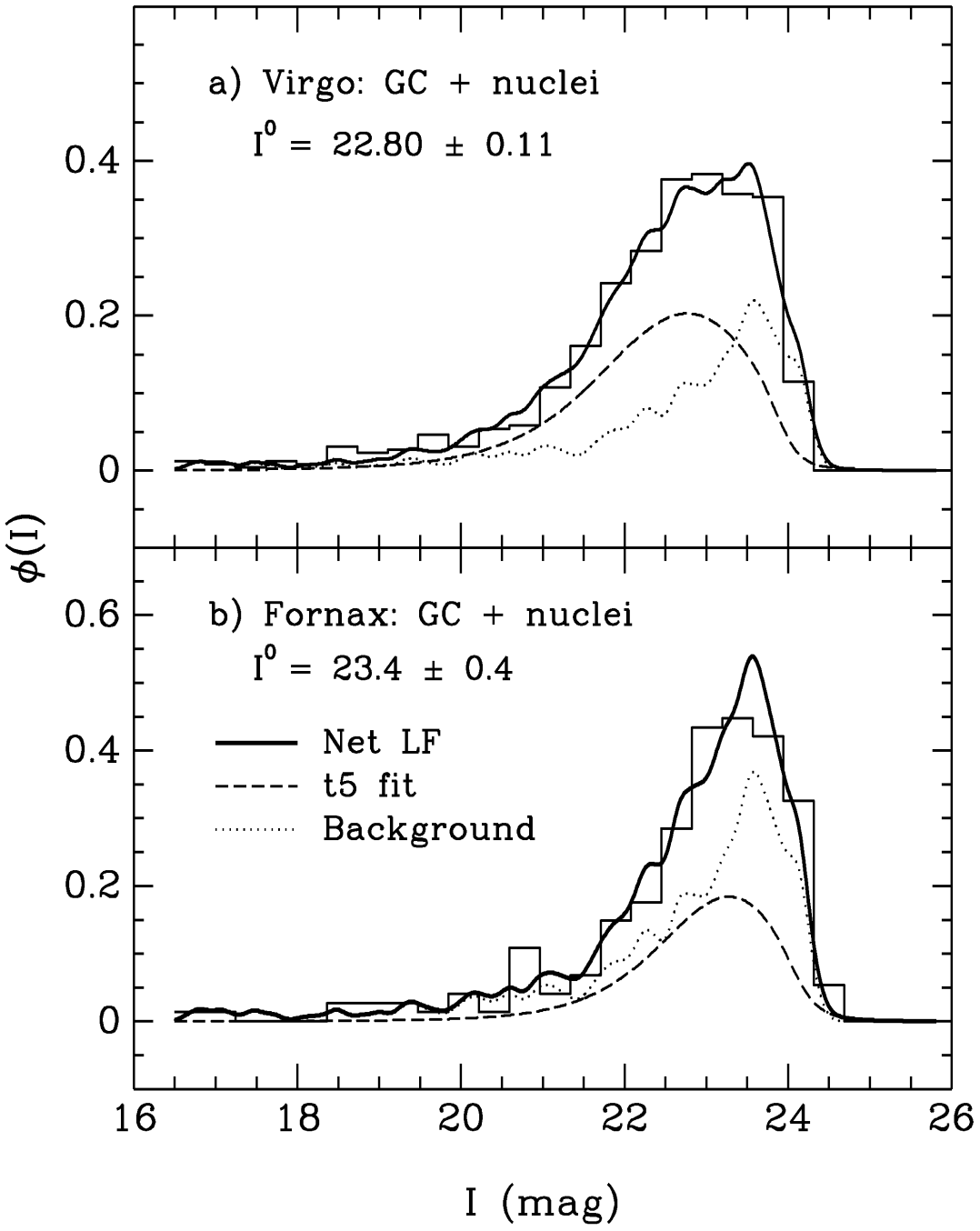

Fig. 3.— I-band GC luminosity functions for the Virgo (a) and Fornax (b) complete samples (GC plus nuclei). The histograms are the LFs for all GC candidates. The dotted curve is the scaled LF of background objects. These values are given in Tables 5. The dashed curve is the best-fitting t_5 distribution using the method of Secker & Harris (1993) and the dark solid curve is the total fit. All the smooth curves have been convolved with the appropriate completeness functions.

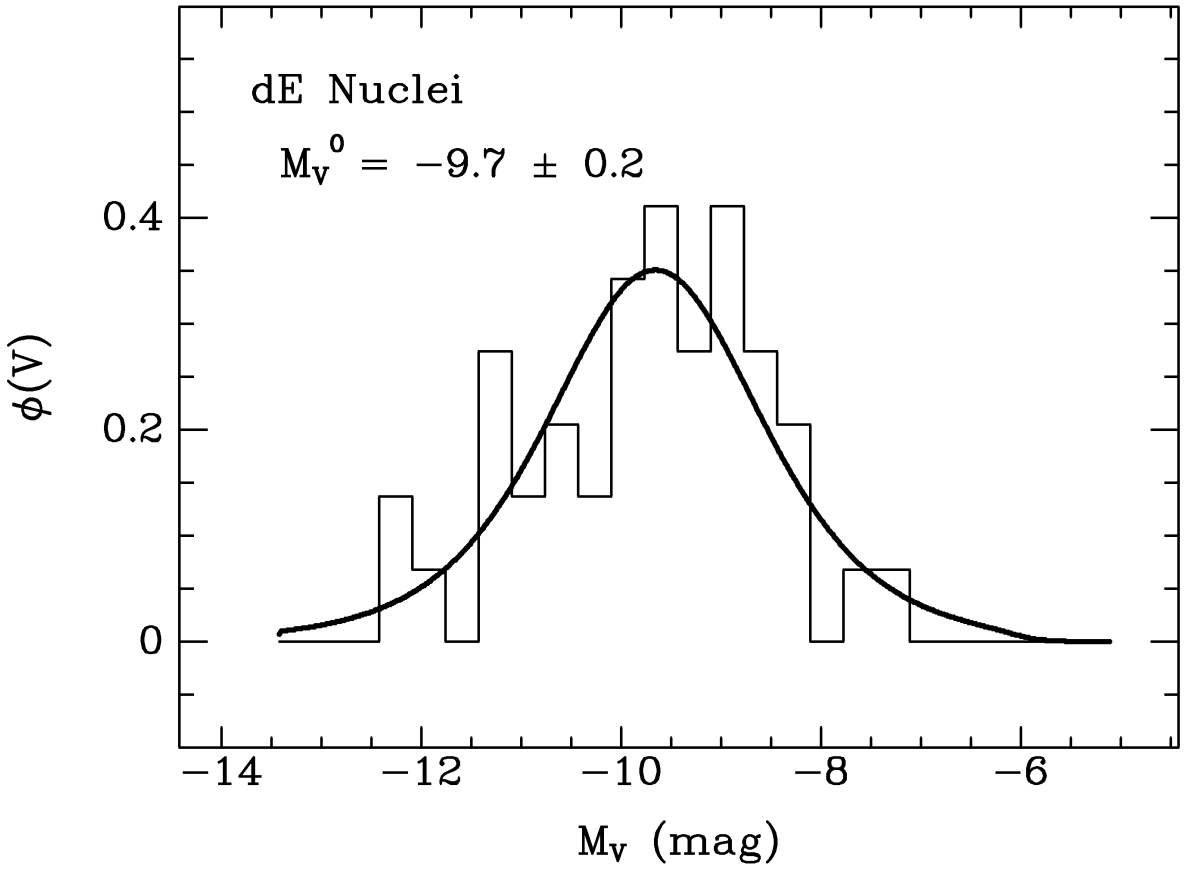

Fig. 4.— V-band luminosity function of the dE nuclei. Since the probability that a bright, compact source near the center of a dE would be a foreground or background source is small, no background subtraction has been done. The solid curve is the best-fitting t_5 function with a peak of $M_V^0 \approx -9.7$ (Table 6).

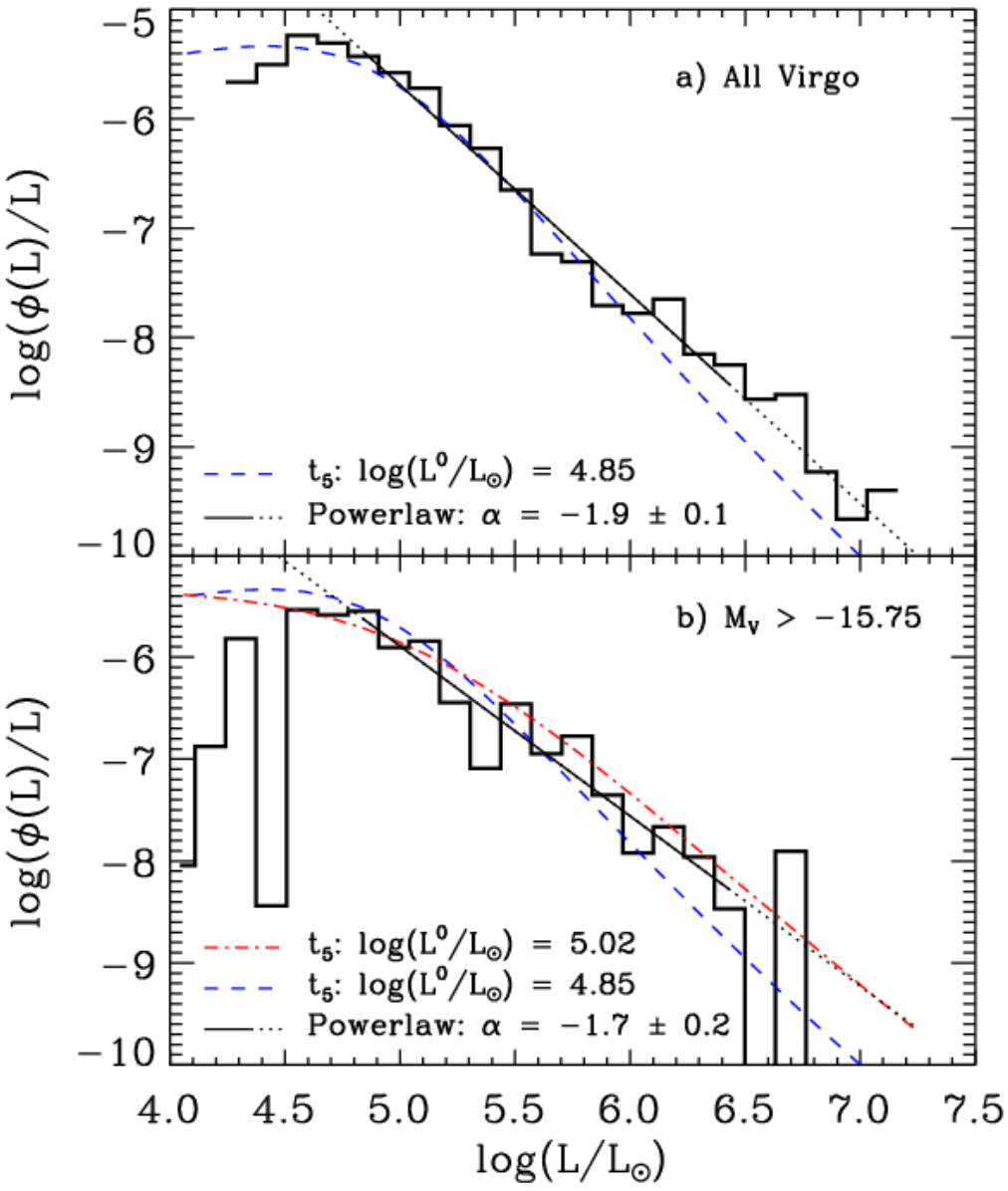

Fig. 5.— Power-law representations of the background-subtracted GCLFs for the GC candidates plus nuclei for the Virgo Cluster sub-sample. a) All galaxies. b) For faint galaxies with $M_V > -15.75$ (see Table 8). The best-fitting t_5 and power-law fits are shown as straight black lines. The power-law fits are made in the interval $4.8 < log(L/L_\odot) < 6.5$ show with the solid straight lines. The dotted straight lines show the extrapolations of the fits. The dashed line is the best-fitting t_5 function to the complete Virgo sample (a). The dash-dot line is the best-fitting t_5 function to the clusters in galaxies with $M_V > -15.75$.

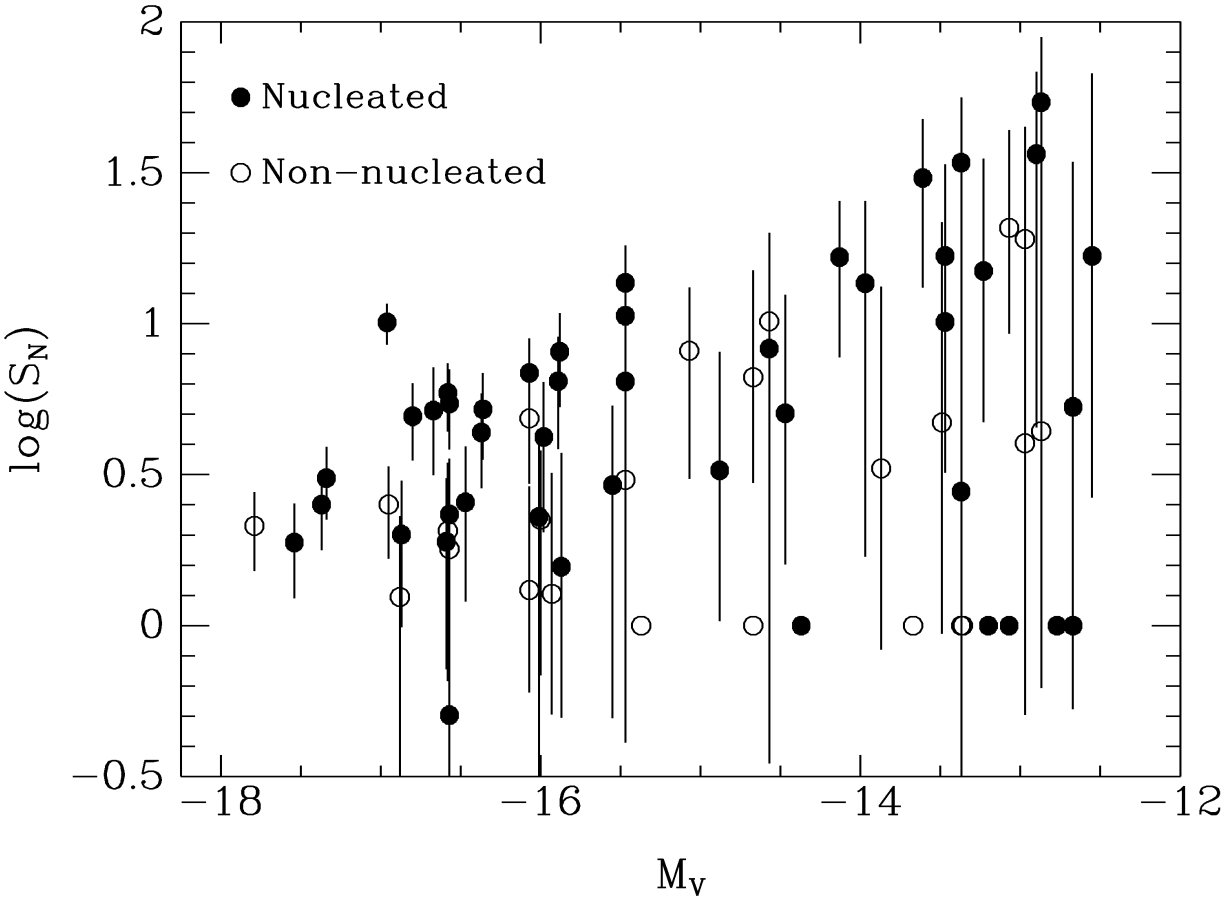

Fig. 6.— $S_{\rm N}$ vs. M_V for the dE,N and dE,noN from the *HST* dE Snapshot Survey. As seen by Miller at al. (1998), $S_{\rm N}$ increases with increasing M_V (decreasing galaxy luminosity). Galaxies with $N_{\rm GC} = 0$ have been given $\log(S_{\rm N}) = 0$ so that they appear on the plot.

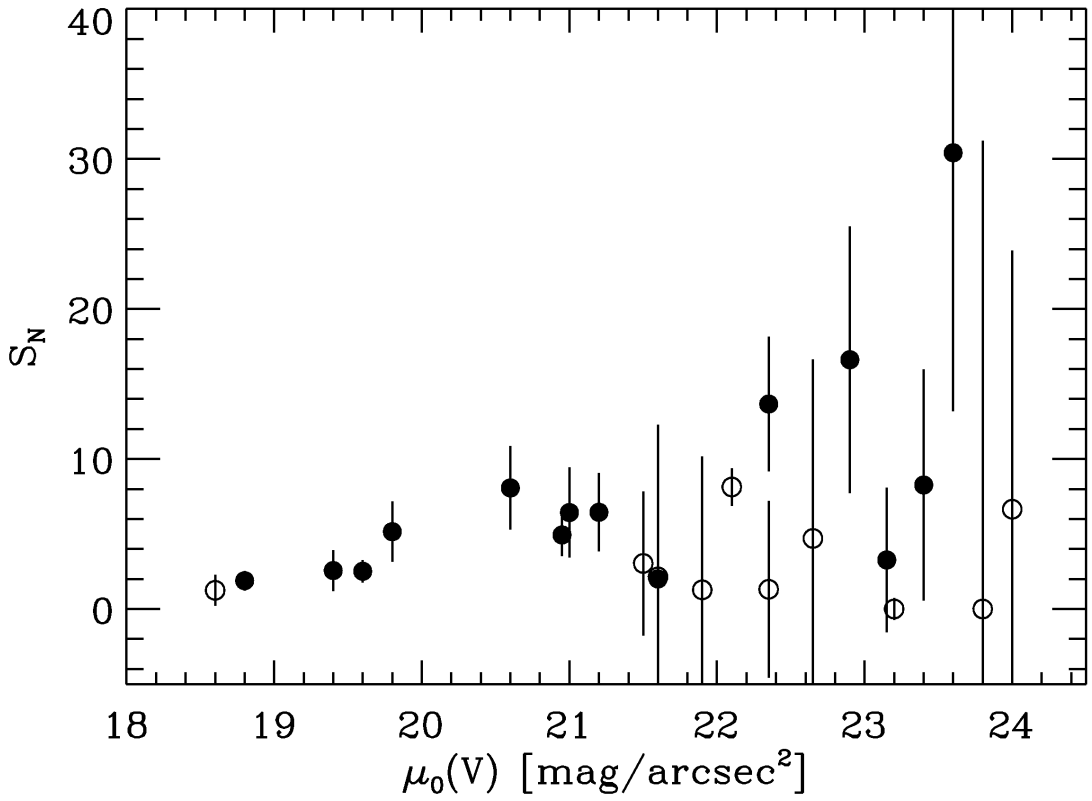

Fig. 7.— S_N vs. central surface brightness for dE,N and dE,noN galaxies. The central surface brightnesses are from the Sersic fits in Stiavelli et al. (2001) in the radial range from 1″ to 5″ and so do not include the nuclei. For the nucleated galaxies S_N increases with decreasing central surface brightness.

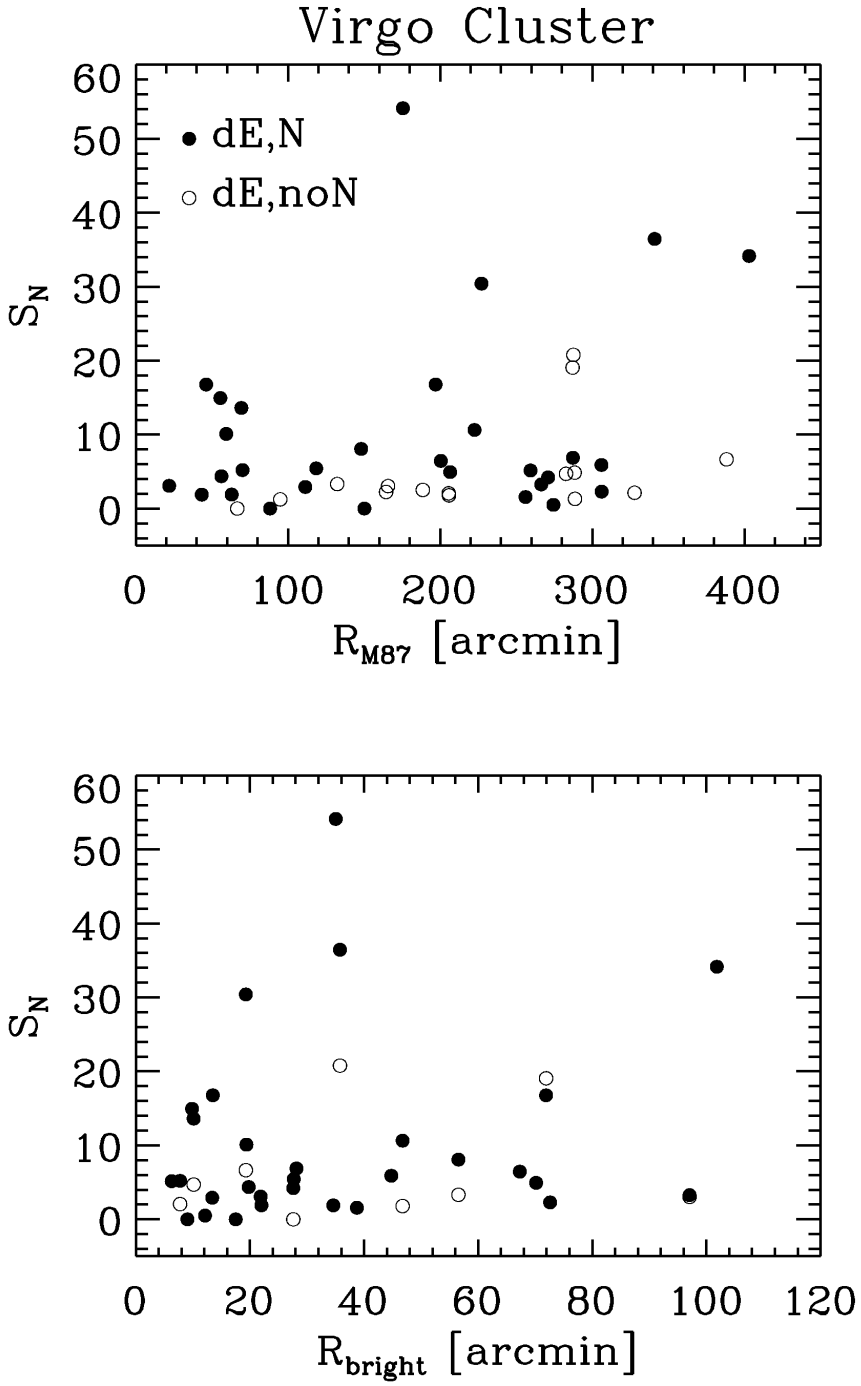

Fig. 8.— S_N versus projected radial distance from M87 (upper panel) and the projected radial distance from the nearest Virgo galaxy with $M_B < -18.6$. There are no clear trends present but in general dE,N always have higher S_N than dE,noN at a given radius.

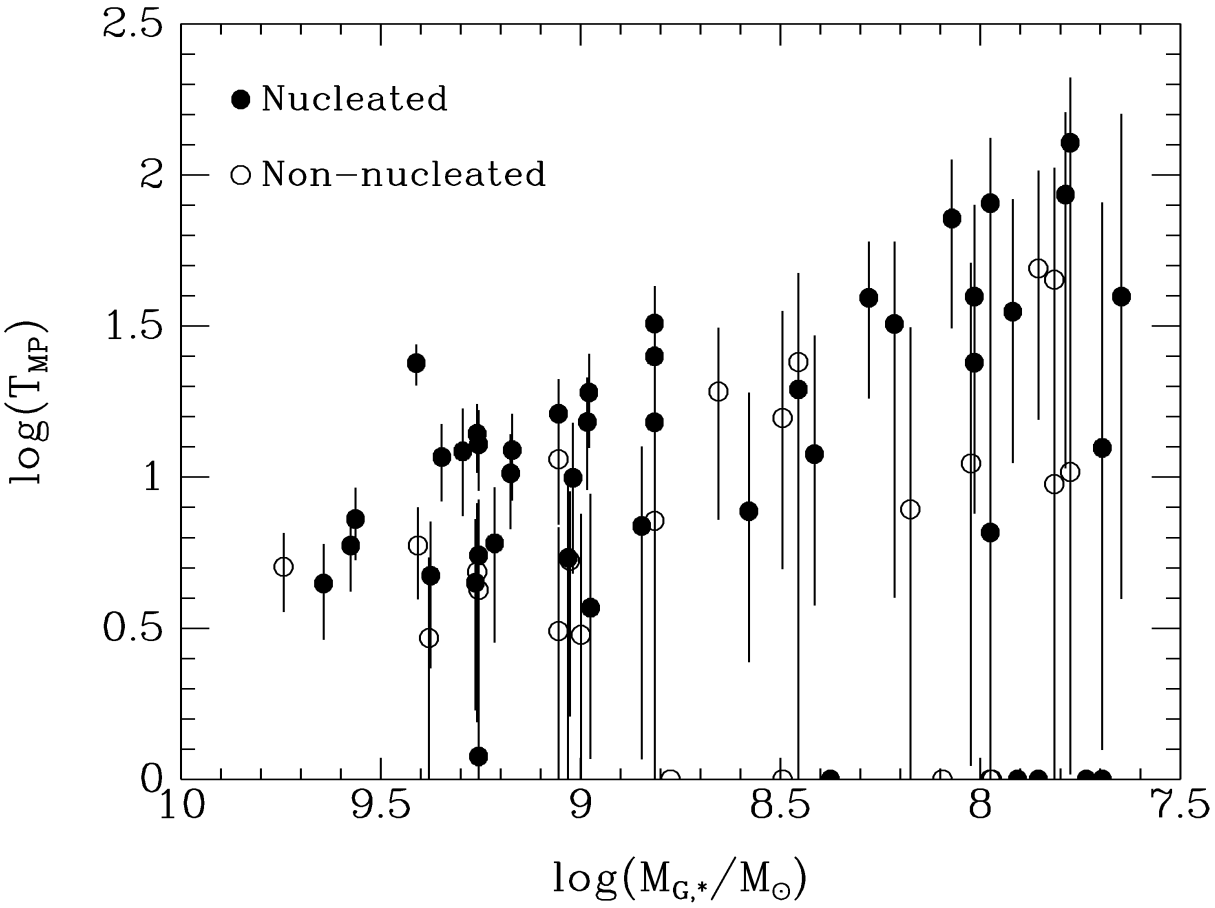

Fig. 9.— $T_{\rm MP}$ vs. $M_{G,*}$ for the dE,N and dE,noN from the *HST* dE Snapshot Survey. As in Figure 6, galaxies with $N_{\rm GC} = 0$ have been given $\log(T_{\rm MP}) = 0$ so that they appear on the plot.

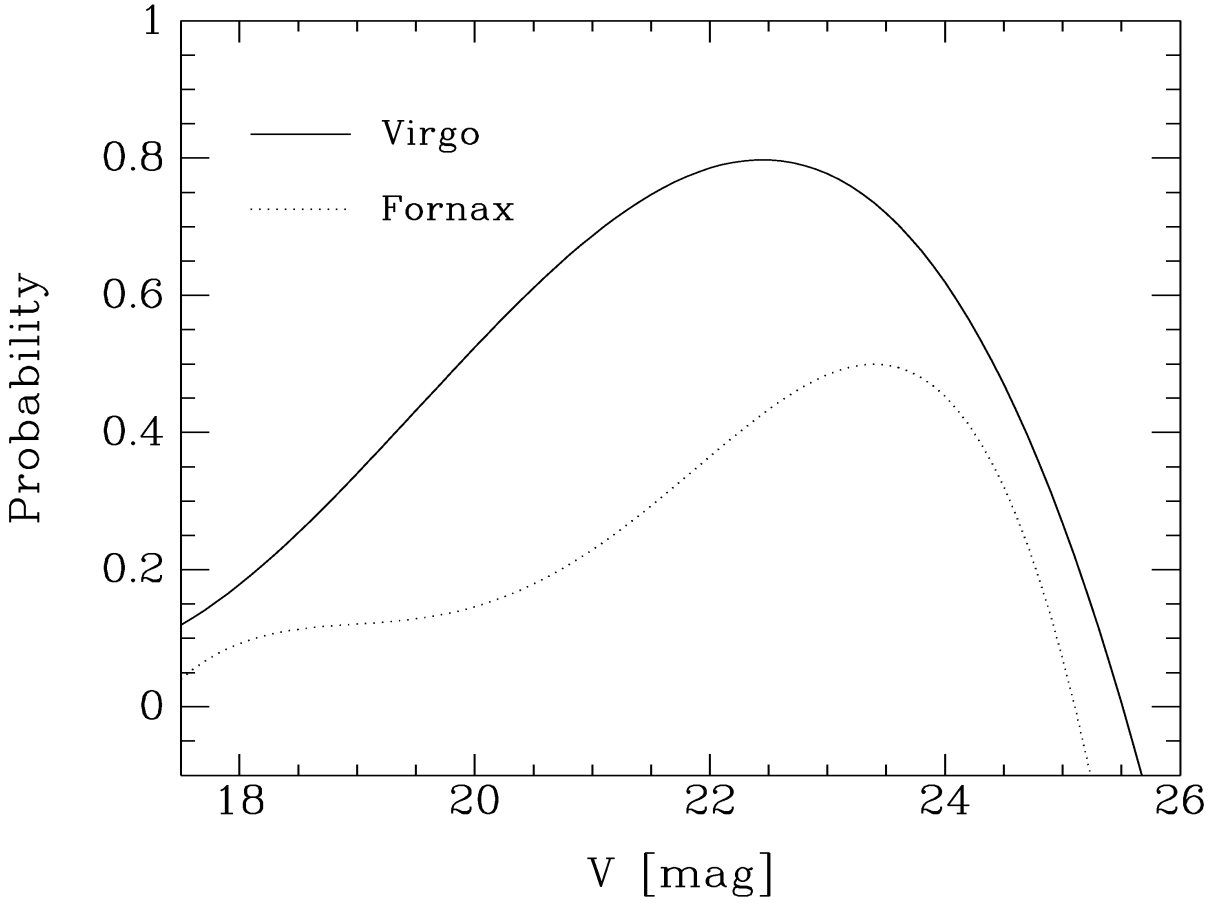

Fig. 10.— Probability with magnitude that a GC candidate in the Virgo Cluster sample of a given apparent magnitude is an actual GC, not a background object.

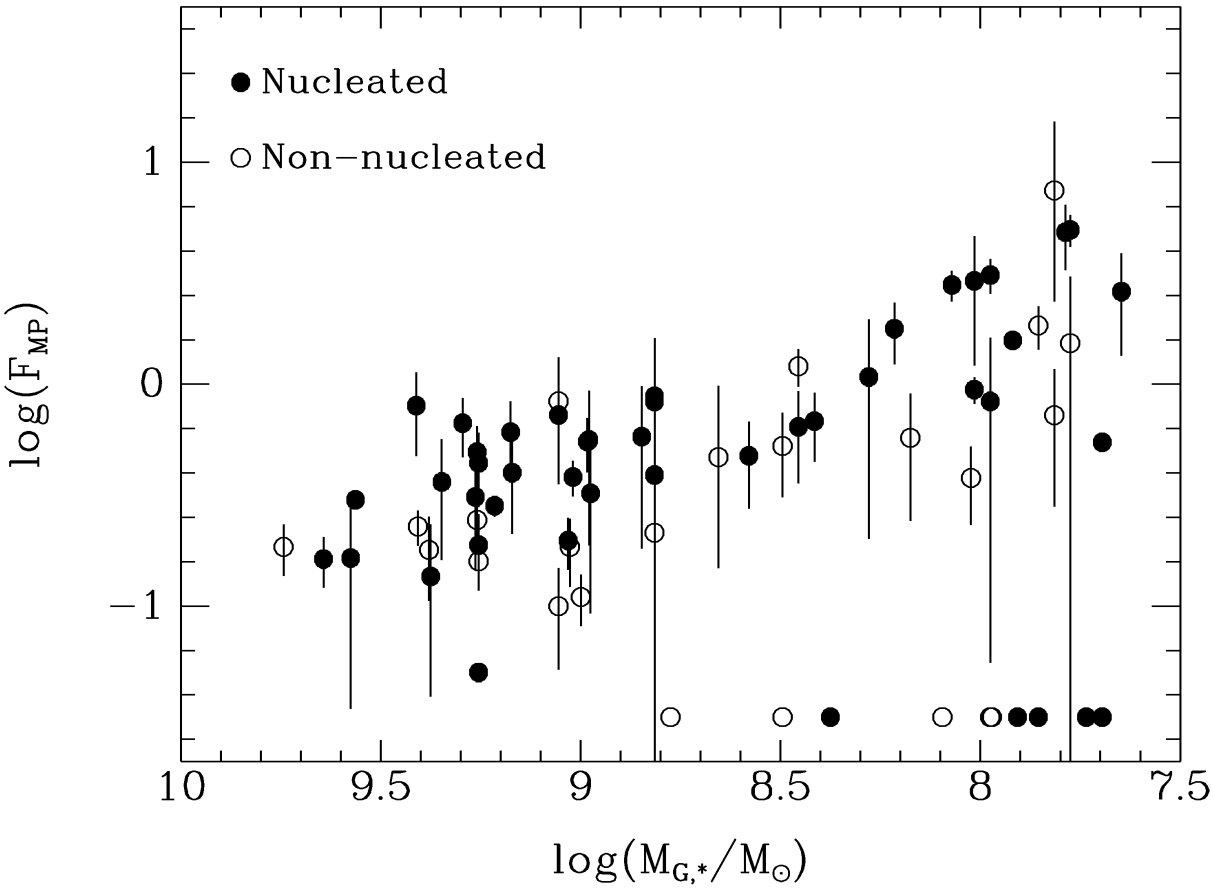

Fig. 11.— $F_{\rm MP}$ vs. $M_{G,*}$ for the dE,N and dE,noN from the *HST* dE Snapshot Survey. Galaxies with $N_{\rm GC} = 0$ have been given $\log(F_{\rm MP}) = -1.5$ so that they appear on the plot.

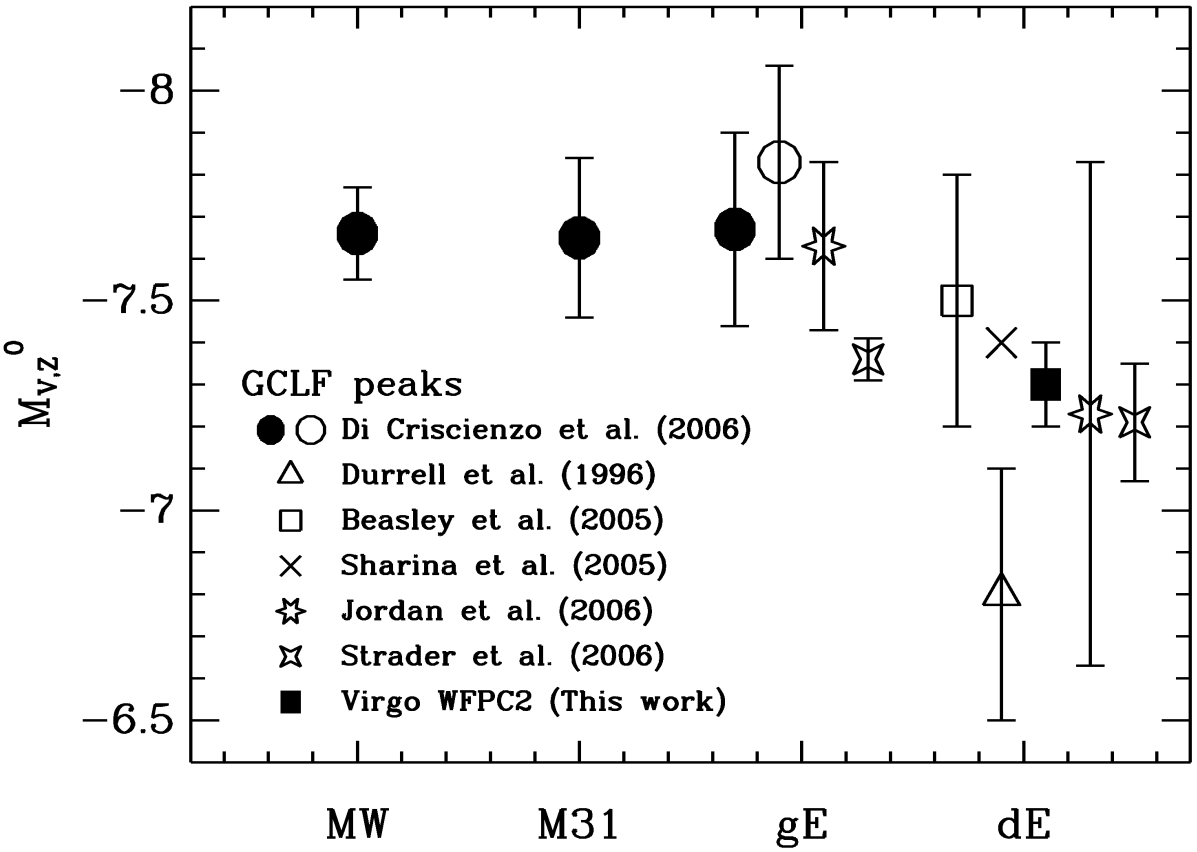

Fig. 12.— Metallicity-corrected GCLF peak magnitudes as a function of host galaxy type. The filled circles are the preferred values from Di Criscienzo et al. (2006) while the open circle represents the GCLF peak for gEs using the Key Project distances (Freedman et al. 2001). The filled square is from the Virgo Cluster sample in this paper and the other points are from the literature (Durrell et al. 1996; Sharina et al. 2005; Beasley et al. 2006; Jordán et al. 2006; Strader et al. 2006) corrected to the Key Project distances where appropriate. While there is significant overlap between the GCLF peak magnitudes in giant and dwarf galaxies, the impression is that on average the GCLF peak in dEs is 0.2–0.5 magnitudes fainter than in giant ellipticals.

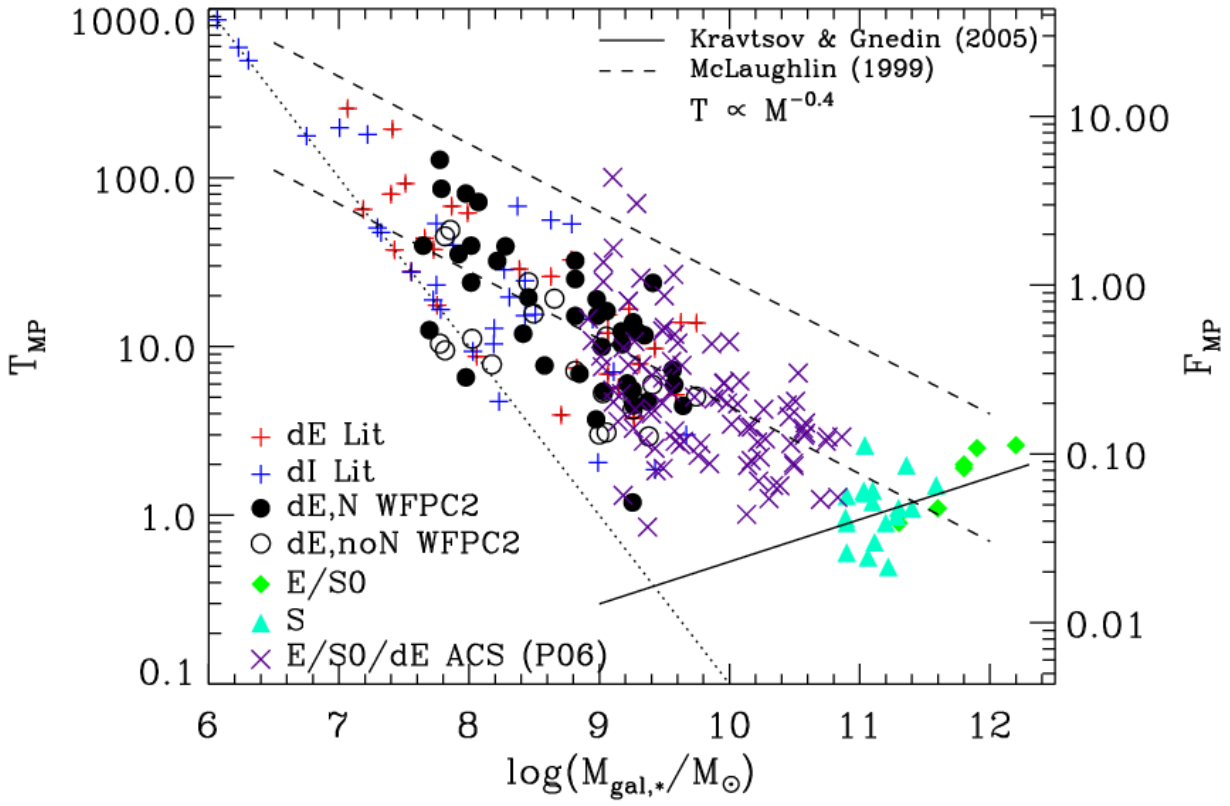

Fig. 13.— The T parameter for metal-poor (MP) GC populations vs. galaxy stellar mass for dE galaxies from the current work and from the literature (see text for references). The equivalent mass fraction, $F_{\rm MP}$, is shown on the right axis assuming a universal GC mass function. The dotted line on the left is the line of constant $N_{\rm GC} = 1$. The solid line is the prediction of $F_{\rm MP}$ with galaxy mass for $\log(M_{G,*}) > 10.5$ from Kravtsov & Gnedin (2005). The dashed lines have a slope of -0.4, from the SNe-driven wind models of McLaughlin (1999). The lower dashed line is the prediction from McLaughlin (1999) for $M/L_V = 5$ for the galaxies. The upper dashed line is an approximation of the upper envelope to the points.